8-1-2018

Spg Directs Arp2/3 Mediated F-actin Networks to Support Syncytial Furrow Ingression in Drosophila

Shannon M. Henry
University of Denver

Spg Directs Arp2/3 Mediated F-actin Networks to Support Syncytial Furrow Ingression in Drosophila

Abstract
In the *Drosophila* embryo, nuclear divisions 10-13 occur in a syncytium with transient membrane furrows separating neighboring nuclei before the occurrence of cellularization. This process is driven by cytoskeletal and membrane trafficking networks, and while RalA and Rab8 have been identified to drive membrane addition to furrows, less is known about the control of dynamic F-actin networks needed for furrow formation. Here, the role of the DOCK protein Sponge (Spg) in furrow formation is explored through shRNA knockdown and live-imaging of syncytial *Drosophila* embryos. I have found that Spg is required for furrow ingression and that without Spg, furrows can only reach 25% of their wild-type length. This is due to a lack of branched F-actin on apical caps and furrows, and Spg is found to be a key regulator in bringing components of the Arp pathway to these structures. Finally, I have demonstrated the requirement for this branched F-actin network in potentiating ingression and linear F-actin networks that are localized along the length of syncytial furrows.

Document Type
Thesis

Degree Name
M.S.

Department
Biological Sciences

First Advisor
Todd Blankenship, Ph.D.

Second Advisor
Michelle K. Knowles, Ph.D.

Third Advisor
Cedric Asensio

Keywords
Drosophila embryo, Syncytial furrow formation

Subject Categories
Biology | Life Sciences

Publication Statement

Spg Directs Arp2/3 Mediated F-actin Networks to Support Syncytial Furrow Ingression

in *Drosophila*

_____

A Thesis

Presented to

the Faculty of Natural Sciences and Mathematics

University of Denver

_____

In Partial Fulfillment

of the Requirements for the Degree

Master of Science

_____

by

Shannon M. Henry

August 2018

Advisor: Todd Blankenship

Author: Shannon M. Henry
Title: Spg Directs Arp2/3 Mediated F-actin Networks to Support Syncytial Furrow
Ingression in *Drosophila*
Advisor: Todd Blankenship
Degree Date: August 2018

Abstract

In the *Drosophila* embryo, nuclear divisions 10-13 occur in a syncytium with

transient membrane furrows separating neighboring nuclei before the occurrence of

cellularization. This process is driven by cytoskeletal and membrane trafficking

networks, and while RalA and Rab8 have been identified to drive membrane addition to

furrows, less is known about the control of dynamic F-actin networks needed for furrow

formation. Here, the role of the DOCK protein Sponge (Spg) in furrow formation is

explored through shRNA knockdown and live-imaging of syncytial *Drosophila* embryos.

I have found that Spg is required for furrow ingression and that without Spg, furrows can

only reach 25% of their wild-type length. This is due to a lack of branched F-actin on

apical caps and furrows, and Spg is found to be a key regulator in bringing components

of the Arp pathway to these structures. Finally, I have demonstrated the requirement for

this branched F-actin network in potentiating ingression and linear F-actin networks that

are localized along the length of syncytial furrows.

Table of Contents

List of Figures

<center>**Introduction**</center>

Overview of the *Drosophila* Syncytial Blastoderm

   The ingression of plasma membrane furrows is a critical process in cellular

systems and is necessary both for initial cleavage cycles and development of tissues as

well as for cytokinesis throughout an organism's lifetime. The syncytial *Drosophila*

embryo serves as a good developmental model for this process, building and

disassembling thousands of furrows on a minutes time scale (Foe and Alberts, 1983;

Holly et al., 2015; Xie and Blankenship, 2018). After fertilization and the formation of

the first diploid nucleus, a rapid series of 9 nuclear divisions occurs deep within the yolk.

However, at division cycle 10 nuclei migrate to form a single layer at the periphery of the

embryo. The subsequent four rounds of division, cycles 10-13, occur in this subcortical

portion of the syncytium before cellularization and the formation of a monolayered

epithelium occurs during cycle 14 (Schejter and Wieschaus, 1993; Mazumdar and

Mazumdar, 2002). To ensure genomic integrity through the syncytial divisions, transient

membrane furrows are formed between neighboring nuclei as they prepare to divide.

These furrows are quickly assembled and disassembled during each cycle 10-13 by

highly coordinated processes involving membrane trafficking and cytoskeletal networks.

My work focuses on the regulation of F-actin networks involved in syncytial furrow

formation.

<center>1</center>

Syncytial Furrow Formation and Dynamics

An important component of *Drosophila* syncytial divisions is the formation of transient membrane furrows. These furrows ingress between neighboring nuclei and partition individual mitotic figures into separate regions, thereby preventing inappropriate chromosomal capture from adjacent mitoses once nuclear membrane breakdown has occurred. Furrows also provide attachment points for mitotic spindles, supporting the machinery that separates chromosomes into bipolar pools (Foe and Alberts, 1983; Sullivan et al., 1993; Holly et al., 2015; Xie and Blankenship, 2018). As nuclei become progressively more densely packed with each successive cycle, furrows grow longer to maintain genomic stability. Furrows initiate at the start of each new cell cycle and reach a maximum depth at metaphase, before retracting back to the embryo cortex during anaphase/telophase in preparation for the start of a new cycle.

The lengthening of syncytial furrows occurs in stages: Ingression I, Stabilization, and Ingression II (Xie and Blankenship, 2018). Early in each cycle, F-actin organizes into a dome-like cap above each nucleus that expands and extends basally as the membrane furrows grow and facilitates centrosome separation (Foe and Alberts, 1983; Sullivan et al., 1993; Cao et al., 2010). Rearrangement of F-actin networks into these dynamic caps is a process that corresponds with the Ingression I stage of furrow formation. Ingression I allows for initial furrow ingression and builds short furrows at a relatively slow rate. While Ingression I is the only furrow ingression mechanism during syncytial cycles 10-11, beginning in cycle 12 a new Ingression II phase follows Ingression I and Stabilization. This phase requires zygotic transcription and possesses a higher ingression rate making it a key contributor to the four-fold increase in furrow length that occurs

from cycles 10-13 (Xie and Blankenship, 2018). To account for this overall increase in length, plasma membrane must be added to the growing furrows. A membrane trafficking pathway centered on RalA, the exocyst complex, and Rab8 mediates exocytic trafficking from the Golgi and apical cell surface required for furrow ingression (Fabrowski et al., 2013; Holly et al., 2015; Figard et al., 2016; Mavor et al. 2016). Beginning in cycle 10, furrow lengthening corresponds to the recruitment of the RalA small GTPase, which is required for localization of the exocyst complex subunit Sec5 to furrows. Together, these proteins recruit Rab8 vesicles to the plasma membrane to direct membrane addition to the furrows (Holly et al., 2015; Mavor et al. 2016). Thus, the regulation and organization of both F-actin and membrane trafficking networks is vital to proper furrow formation (Sokac and Wieschaus, 2008; Fabrowski et al., 2013; Figard et al., 2016).

Actin Nucleation and Regulation

While much of the membrane trafficking pathway involved in furrow formation has been uncovered, less is known about the role cytoskeletal rearrangements play in this process. Actin can exist either as monomers (G-actin) or filaments (F-actin), and often cycles between these two states. F-actin is characterized by a slow-growing minus end and a fast-growing plus end, and these filaments are involved in many cell processes including structural support, cell migration, and contraction. Two populations of F-actin are involved in syncytial furrow formation: linear F-actin mediated by members of the Formin family of proteins, and Arp2/3 mediated branched F-actin. Each of these populations are distinct but closely related in the syncytial embryo, and both are required for proper furrow ingression.

Linear F-actin is strongly associated with ingressing furrows and is directed by Diaphanous (Dia), the main Formin in *Drosophila*. Dia is a highly conserved protein with F-actin nucleating and elongating behavior activated by the GTPase Rho1. This activity can be regulated by an autoregulatory domain within Dia which can interact with the Rho binding domain to prevent binding to active Rho1 (Bogdan et al., 2013). In *Drosophila*, Dia has been found to be important for filopodial-driven migration events, Clathrin-mediated endocytosis, furrow ingression during syncytial divisions and cellularization, and bundling of apical F-actin during cap expansion (Afshar et al., 2000; Cao et al., 2010; Bogdan et al., 2013). When Dia function is disrupted, furrows fail to ingress fully during syncytial stages and cellularization (Afshar et al., 2000).

Branched F-actin in syncytial stages is more strongly associated with the dome-like caps that form above each nucleus from cycle 10-13. This population of Actin is directed by the Arp2/3 complex and its many regulators. The Arp2/3 complex is made up of two Actin-related proteins (Arp2 and Arp3) along with five other subunits and can be found in all eukaryotes. This complex binds to actin filaments to promote polymerization and cross-linking, and can establish new branches off of existing filaments classically at 70° angles (Machesky and Gould, 1999; Daly, 2004). Branched Arp2/3 F-actin networks have been implicated in lamellipodial-driven migration, and in the early *Drosophila* embryo as an important factor for apical cap expansion and furrow ingression (Stevenson et al., 2002). By itself, Arp2/3 nucleation activity is relatively low, but can be regulated and enhanced by several factors. Most notable of these factors are the WASp and Scar/WAVE family proteins, which are activated by the GTPase Rac1 and bind both monomeric Actin and Arp2/3 to promote nucleation. While Wasp does not play any

major role in the *Drosophila* blastoderm, Scar has been found to be crucial to forming full-sized Actin caps and furrows (Zallen et al., 2002). Another protein that promotes Arp2/3 activity is Cortactin, which binds F-actin and Arp2/3, thereby bringing Arp2/3 to established filaments off of which it can more effectively polymerize Actin and begin new branches. Actin branchpoints can additionally be stabilized by Cortactin (Daly, 2004). In *Drosophila* syncytial embryos, Cortactin has been shown to be associated with Actin caps and furrows (Rikhy et al., 2015). Another F-actin binding protein in *Drosophila* is Coronin, a member of the Coronin family which is known to promote Actin polymerization, cytokinesis, and other Actin-dependent processes (Bharathi et al., 2003). Coronin is highly expressed throughout *Drosophila* development, and in yeast, directly regulates Arp2/3 (Rybakin and Clemen, 2005). A second subset of Coronin family proteins includes *Drosophila* Dpod1, which crosslinks F-actin and microtubules and can be found on syncytial caps and furrows (Rothenberg et al., 2005; Rybakin and Clemen, 2005).

Collectively, these proteins are important to the formation and regulation of F-actin networks in the early *Drosophila* embryo, and therefore may play a role in the cytoskeletal rearrangements necessary for furrow formation.

Functions of the Sponge Protein

Sponge (Spg) is a large ~2002 amino acid protein containing SH3, DHR, Armadillo helical repeat, and DOCK domains, and is the *Drosophila* homolog of mammalian DOCK-B family Rho GEFs. DOCK proteins are Rho GEFs unique in the fact that they lack the Dbl homology domain common to most GEFs. These proteins

primarily activate Rac1 and Cdc42, and function in a variety of processes including cell migration, phagocytosis, myogenesis, and neurogenesis (Côté and Vuori, 2007; Gadea and Blangy, 2014; Laurin and Côté, 2014). The DOCK-B family consists of Dock3 and Dock4, which are mainly implicated in cytoskeletal remodeling during neurogenesis (Laurin and Côté, 2014). Disruptions in Dock3 have been shown to lead to irregular axonal development causing developmental disabilities, hypotonia, and gait ataxia (Helbig et al., 2017; Iwata-Otsubo, 2017). Dock4, which is unique from other DOCK proteins in that it can activate Rap1 in addition to Rac1 and Cdc42, is important to dendrite development and is mutated in several human cancer cell lines (Yajnik et al., 2003; Ueda et al., 2008).

In *Drosophila* development, Spg has been shown to function as a Rap1GEF necessary for proper axonal outgrowth (Biersmith et al., 2011), dorsal vessel patterning (Biersmith et al., 2015), and R7 photoreceptor differentiation (Eguchi et al., 2013). Spg has also been shown to act as a Rac1GEF, notably in thorax development (Morishita et al., 2014). During syncytial stages, Spg has been implicated in actin cap formation, with *spg* mutants lacking these structures and consequently having high rates of chromosomal missegregation beginning in cycle 11 (Postner et al., 1992; Sullivan et al., 1993).

Thesis Specific Aims

The goal of this thesis is to understand Spg and F-actin function at apical caps and during furrow ingression. To do this, live-imaging and immunostaining techniques were used to visualize Spg, F-actin, and critical F-actin regulators in syncytial embryos. Furrow length and ingression dynamics were measured and compared between wild-type

6

embryos and embryos lacking Spg, Diaphanous, or Arp2/3 by shRNA knockdown to determine which of these components are important for furrow ingression. Additionally, the ability to form apical caps in these backgrounds was compared by measuring cap area, and the role of Spg in cap formation was explored by measuring localization and intensity of Arp2/3 regulators on these caps in both wild-type and *spg* shRNA backgrounds. These data have allowed a proposed mechanism of Spg function in the *Drosophila* syncytial blastoderm to be uncovered.

Methods

Fly Stocks and Genetics

      Fly stocks were maintained at 25°C by standard procedures. All UAS transgenic flies were crossed with matαTub-Gal4VP16 67C;15 maternal driver females (D. St Johnston, Gurdon Institute, Cambridge, UK), and second-generation embryos were analyzed. The following fly stocks were used in this study: Oregon R BL-5, His2Av:RFP BL-23650 and BL-23651, Spg Valium22 BL-35396, UASp-YFP:Rab8 BL-9782, UASp-Arpc1:GFP BL-26692, Arpc4 Valium20 BL-41888, Dia Valium22 BL-35479, Rac1 Valium20 BL-34910, Rac1:GFP BL-52285, and Rap1 Valium20 BL-57851 were obtained from the Bloomington Stock Center, and Gap43:mCh (A. Martin, MIT), spg805 and spg242 alleles (E. Wieschaus, Princeton), Resille:GFP (A. Spradling, Carnegie Institution), UASp-RalA:GFP (Blankenship lab), UASp-MoeABD:mCh (T. Millard, University of Manchester), UASp-Cortactin:GFP (Blankenship lab), UASp-DPod1:GFP (Blankenship lab), UASp-Scar:GFP (Blankenship lab), UASp-Coronin:GFP (Blankenship lab), and Rap1:GFP (N. Brown, Cambridge University).

Microscopy and Time-Lapse Imaging

Fixed images were acquired with an Olympus Fluoview FV1000 confocal laser scanning microscope with a 60×/1.42NA objective for fixed specimens. Time-lapse imaging was performed on a spinning-disk confocal microscope from Zeiss/Solamere Technologies Group with 63X/1.4NA objective lens. Embryos were collected on standard yeasted apple juice agarose plates, dechorionated, and transferred to a gas-permeable membrane in Halocarbon 27 oil (Sigma). A coverslip was placed on embryos for live imaging. Fixed specimen imaging was performed using 4-10 µs/pixel exposure settings, and live imaging was performed using 150-200 ms exposure times. For individual time-lapse imaging, full z-stacks were acquired at 30s intervals. Each z-stack was comprised of 30–33 z-slices at a 0.5 µm interval. All movies were acquired at 25˚C.

Embryo Fixation and Immunostaining

Embryos were dechorionated in 50% bleach solution and fixed for 1hr to 1hr 15min at the interface of heptane and 3.7% formaldehyde in 0.1 M sodium phosphate buffer (pH 7.4) before being manually devitellinized and stained with Alexa 568-phalloidin (1:500; Molecular Probes), guinea pig anti-Spg (1:500; Biersmith et al., 2011), rabbit anti-GFP (1:1000; Invitrogen, A11122), or mouse anti-GFP (1:100; Molecular Probes, A11120). For anti-Dia stains, embryos were dechorionated in 50% bleach solution and fixed for 5-15 min at the interface of heptane and 3.5% formaldehyde in 0.1 M sodium phosphate buffer (pH 7.4). Embryos were devitellinized by vigorously shaking in a 1:1 solution of heptane and methanol for 1 minute. Embryos were washed 3 times with methanol over an hour and rehydrated in successive solutions of 70%, 50%, 30%,

and 10% methanol in PBS, and then in PBS alone. Embryos were stained with rabbit anti-Dia FH2 domain (1:5000). Secondary antibodies conjugated with Alexa 488 or Alexa 568 (Molecular Probes) were used at 1:500. Embryos were mounted in ProLong Gold with DAPI staining (Life Technologies).

Furrow Dynamics Measurements

Furrow cycle dynamics were measured by live-imaging embryos with both membrane and histone markers. The first, apical z-layer of the furrow was determined as the point at which the apical membranes meet and come to a common width (Xie and Blankenship, 2018). Furrow ingression was tracked by determining the first moment that intact furrow rings comprising a 4–5 "cell" region had advanced to a new basal layer. Maximal ingression rates were calculated from a 2-minute rolling window during each ingression phase.

Furrow widths were measured by hand with the ImageJ straight line tool. For each furrow measured, a straight line was drawn across the entire width of the furrow (edge to edge) at the "top", "middle", and "bottom" of the furrow. 6 furrows were measured for each ingression phase, at the following representative cycle time points and z-layers. Cycle 10: 2 min, 0.5 µm. Cycle 11: 4 min, 1 µm. Cycle 12, ingression I: 2 min, 1 µm. Cycle 12, ingression II: 9 min, 1 µm. Cycle 13, ingression I: 2 min, 1 µm. Cycle 13, ingression II: 12 min, 1 µm.

Apical Cap Measurements

Actin cap area and cap protein intensity levels were measured by live-imaging wild-type and *spg* shRNA, *dia* shRNA, *arpc4* shRNA, or *rac1* shRNA embryos expressing either MoeABD:mCh, Arpc1:GFP, Cortactin:GFP, DPod1:GFP, Scar:GFP, or Coronin:GFP under identical acquisition settings. In each cycle 10-13, the image at a time-point of 2 min after the start of cap formation and a z-layer 0.5 µm from the most apical point of the cap was analyzed. 6 caps were selected and each was hand-traced 3 times with the ImageJ freehand selection tool. For Arpc1:GFP in the *spg* shRNA background, due to having no visible cap-like structures, cap traces from corresponding wild-type images were transferred onto *spg* shRNA images and placed 1 µm apical of nuclei. ImageJ measurements of area, mean gray value, and integrated density were taken, and the mean area was calculated for each cycle. Background fluorescence was analyzed by measuring 6 cytoplasmic areas in the same z-layer and time point that caps were measured. For each individual measurement of the cap, the average of the mean gray values from cytoplasmic areas was multiplied by the area of the cap. This value was subtracted from the cap integrated density, and the resulting difference was divided by the area of the cap. This value was recorded as the true fluorescence intensity corrected for background noise, and the mean value for each cycle was calculated.

Furrow Intensity Measurements

Furrow protein intensity levels were measured by live-imaging wild-type and *spg* shRNA embryos expressing either RalAGFP, MoeABDmCh, Rac1GFP, or Rap1GFP under identical acquisition settings, or imaging wild-type, *spg* shRNA, *dia* shRNA, or

spg/dia shRNA embryos immunostained with anti-Dia or Phalloidin under identical acquisition settings. For live-imaging, in each cycle 10-13, the image at a time-point of 4 min after the start of furrow formation and a z-layer 1 µm from the most apical point of the furrows was analyzed. For fixed imaging, a z-layer 1 µm from the most apical point of the furrows was analyzed and data from all images were pooled as accurate time points could not be determined. Furrows were hand-traced using the ImageJ freehand line tool, tracing the furrow around the entire perimeter of a "cell". 6 sets of furrows were selected and hand-traced 3 times. ImageJ measurements of area, perimeter, mean gray value, and integrated density were taken, and the mean area was calculated for each cycle. Background fluorescence was analyzed by measuring 6 cytoplasmic areas in the same z-layer and time point that furrows were measured. For each individual furrow measurement, the average of the mean gray values from cytoplasmic areas was multiplied by the area of the furrow trace. This value was subtracted from the furrow integrated density, and the resulting difference was divided by the area of the furrow trace. This value was recorded as the true fluorescence intensity corrected for background noise, and the mean value for each cycle was calculated.

Particle Measurements

Rab8 particle count and area were measured by live-imaging wild-type and *spg* shRNA embryos expressing YFP:Rab8 under identical acquisition settings. In each cycle 10-13, the image at a time-point of 2 min after the start of the cycle and a z-layer containing maximal Rab8 particles was analyzed. These criteria were chosen as opposed to a common z-level because Rab8 localization corresponds to furrow depth, and

identical z-levels between wild-type and *spg* shRNA images would therefore have inherent differences in Rab8 localization due to vastly different furrow lengths. Each image was leveled in ImageJ to optimally show Rab8 compartments over cytoplasmic background noise, and a Gaussian blur (σ=1.0) was applied. The image was then converted to a binary. A square area of uniform size was selected and the ImageJ Analyze Particles tool was used to count particles within that area and measure the area of each. This was repeated for 4 areas per image. The mean particle area for each cycle was calculated, as well as the overall size distribution in each cycle by categorizing particles into bins of 0.2 μm^2. To account for variability in number "cells" as *spg* knockdown leads to errors in nuclear division, the particle count for each area was divided by the number of nuclei from the original image that fit within the uniform square area.

Statistics and Repeatability

Furrow length, width, and ingression rate, Rab8 particle count and size, protein intensity on apical caps and furrows, and apical cap area data were tested for statistical significance using Student's t-test. ns: $p>0.05$; *:$p<0.05$; **: $p<0.01$; ***: $p<0.001$. All measurements were quantified from a minimum of 3 embryos, and represented at least two individual trials.

Image Editing and Figure Preparation

Spinning disk and laser scanning confocal microscopy images were edited using Adobe Photoshop. Images were uniformly leveled for optimal channel appearance.

Furrow dynamics curves were made in OriginLab. Figures were prepared and labeled in

Adobe Illustrator.

Results

Sponge is required for furrow ingression

Previous studies have focused on the contributions of membrane trafficking networks to the formation of cytokinetic-like cleavage furrows in the early *Drosophila* embryo. Here, we focus on the contributions of the filamentous actin cytoskeleton in supporting furrow ingression. A convenient tool to perturb F-actin function is the *sponge* mutant. Sponge localizes to syncytial furrows (Fig. 1A), and defects in Sponge function lead to massive disruptions of F-actin distributions in the early embryo (Postner et al., 1992; Sullivan et al., 1993). Given this level of F-actin disruption, we wanted to see the degree to which furrow behaviors still occurred. Careful measurements of furrow dynamics indicated that while wild-type furrows reach depths of about 8 µm by cycle 13, furrows in *sponge* mutant embryos reach only a maximum of approximately 2 µm (Fig. 1B-C). Interestingly, these shortened furrows show clear ingression and stabilization phases during each cycle, suggesting Spg may be a common regulator of furrow formation rather than only affecting individual phases of furrow ingression (Fig. 1C, E-F). Similar results were acquired using *spg* shRNA tools; furrow ingression in each cycle follows a wild-type biphasic pattern, but furrows only reach a maximum length of about 2 µm as in *spg* mutants (Fig. 1 B-F). Because of this, we determined that the *spg* shRNA

phenotype is representative of a true *spg* loss-of-function phenotype and used *spg* shRNA embryos for all further experiments.

One explanation for the severely shortened furrows in *spg* backgrounds could be that *spg* disruption may cause cell cycle defects, and since furrows form transiently during each nuclear division cycle there may be inadequate time to build furrows in *spg* embryos. However, cell cycle time is unaffected by *spg* disruption (Fig. 1 D), further indicating the phenotype is likely due to the inability of core machinery to build furrows. These results demonstrate that Spg function is required for syncytial furrows to ingress longer than a few microns in length.
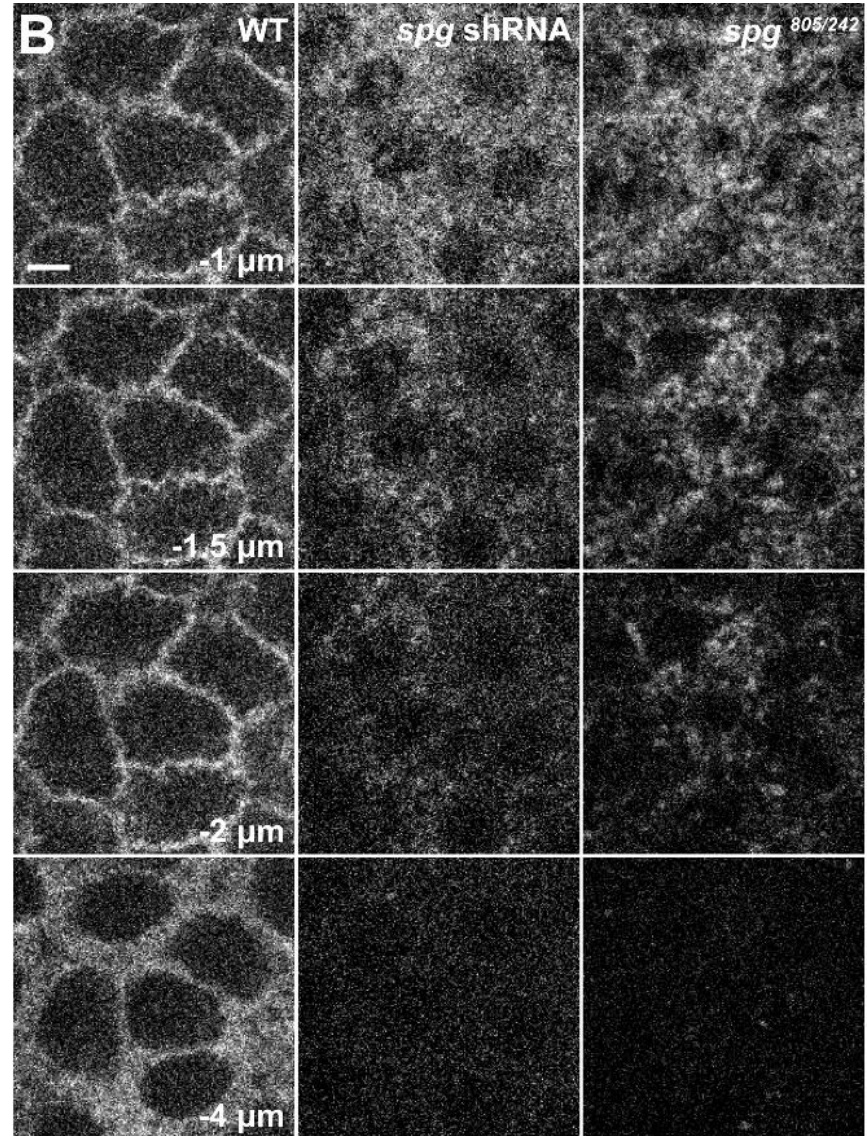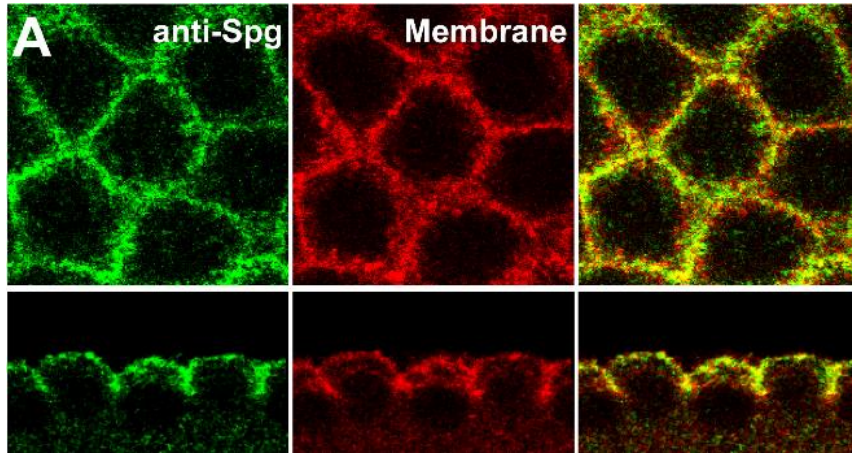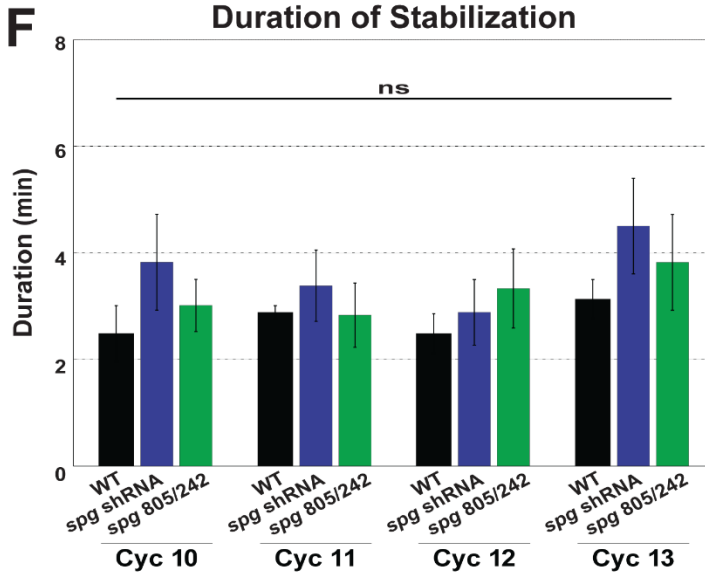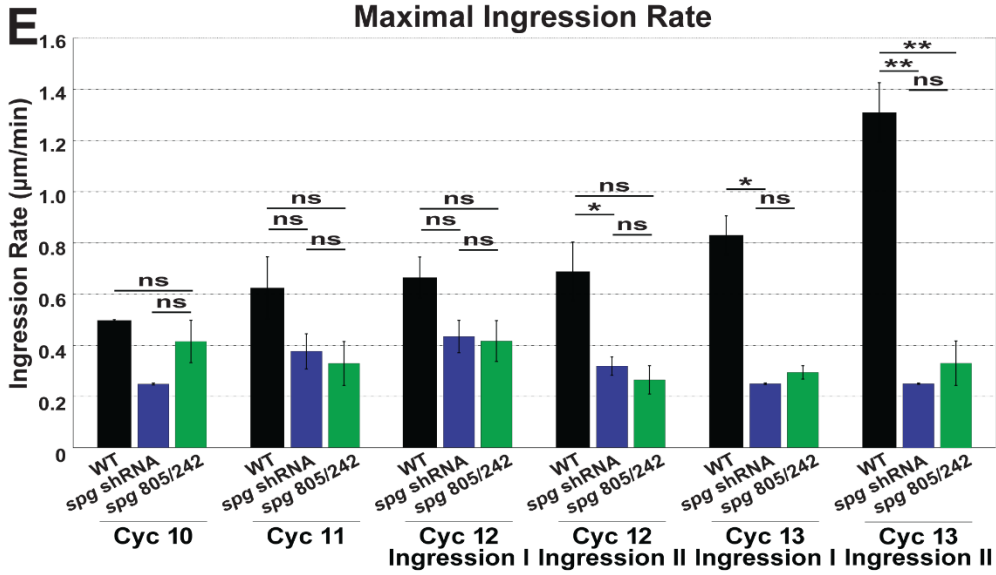
Figure 1. Spg is required for syncytial furrow ingression.
(A) Immunostaining for Spg (green) and plasma membrane
(red) during syncytial cycle 12 shows top-down and side
views of furrows. (B) Still images from live-imaging furrow
dynamics at t=4 min in cycle 12. Scale bar=5 μm.
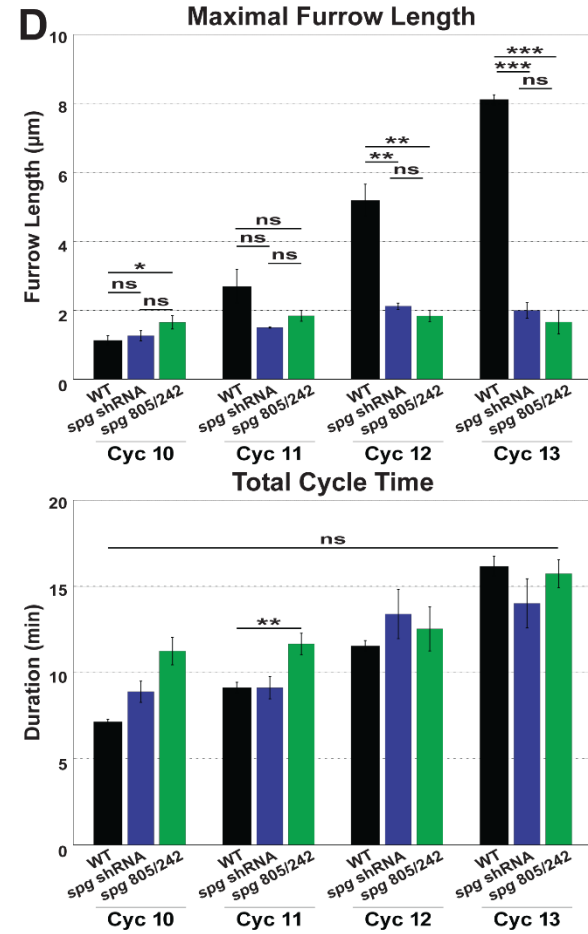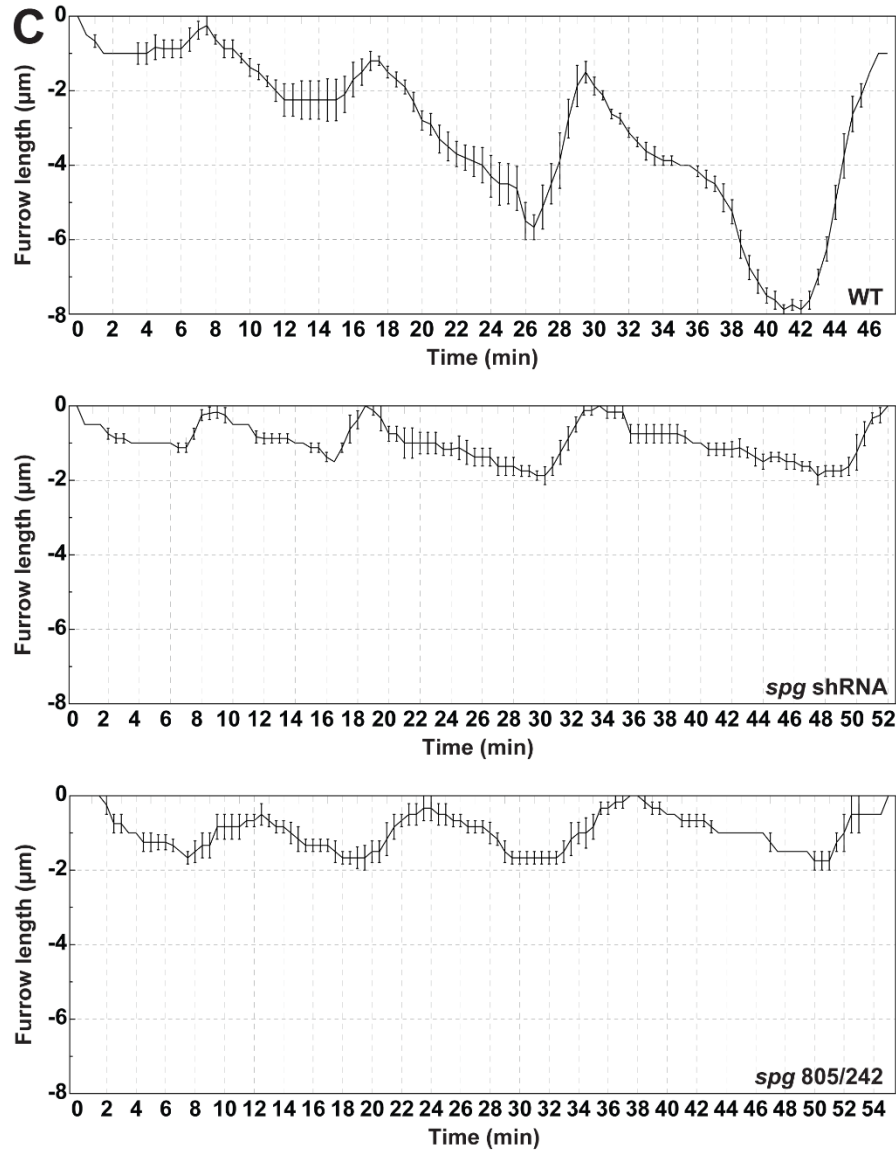
Figure 1 cont. Spg is required for syncytial furrow ingression. (C) Biphasic furrow ingression dynamics in wild-type, spg shRNA, and spg mutant embryos from cycle 10-13. (D) Maximal furrow length and total cycle time from cycle 10-13.

18

Figure 1 cont. Spg is required for syncytial furrow ingression. (E) Maximal furrow ingression rate from cycle 10-13 Ingression I and Ingression II in wild-type and *spg* embryos, calculated from a 2-minute rolling window. (F) Duration of the Stabilization phase of each cycle 10-13 in wild-type and *spg* embryos.

Sponge does not affect membrane trafficking protein distributions

To rule out the possibility that Spg works primarily in the membrane trafficking network to promote furrow formation, we observed two major components of this network, Rab8 and RalA, in *spg* disrupted embryos. In syncytial stages, Rab8 is present in numerous compartments that localize dynamically to the ingressing membrane (Mavor et al., 2016). These dynamic compartments were seen in both wild-type and *spg* embryos (Fig. 2A), and differences in quantity or compartment sizes were insignificant (Fig. 2B-C). Similarly, RalA localized properly to the plasma membrane furrows in both wild-type and *spg* embryos in similar amounts, as indicated by fluorescence intensity (Fig. 2D). The comparatively wild-type behavior of Rab8 and RalA when *spg* is disrupted suggests that Spg is not involved in membrane trafficking pathways and may instead be involved in furrow formation through cytoskeletal networks.
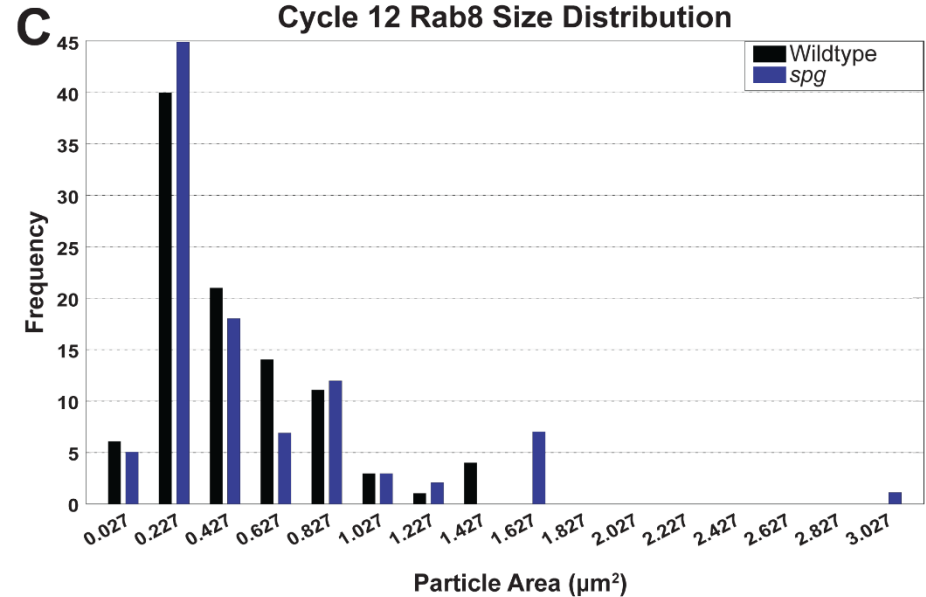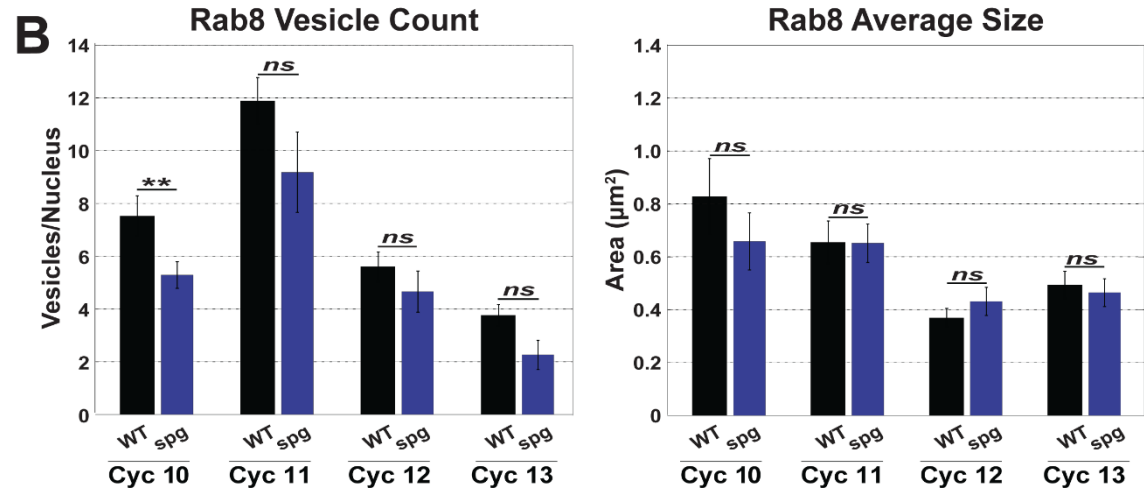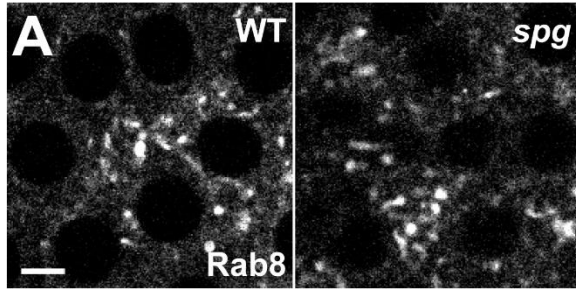
Figure 2. Spg does not affect membrane trafficking pathways. (A) Still images from live-imaging Rab8 at t=2 min in cycle 12 of wild-type and *spg* embryos. Scale bar=5 µm. (B) Quantity of Rab8 compartments (left) and average size of compartments (right) from cycle 10-12 in wild-type and *spg* embryos. (C) Size distribution of Rab8 compartments from cycle 10-13 in wild-type and *spg* embryos.
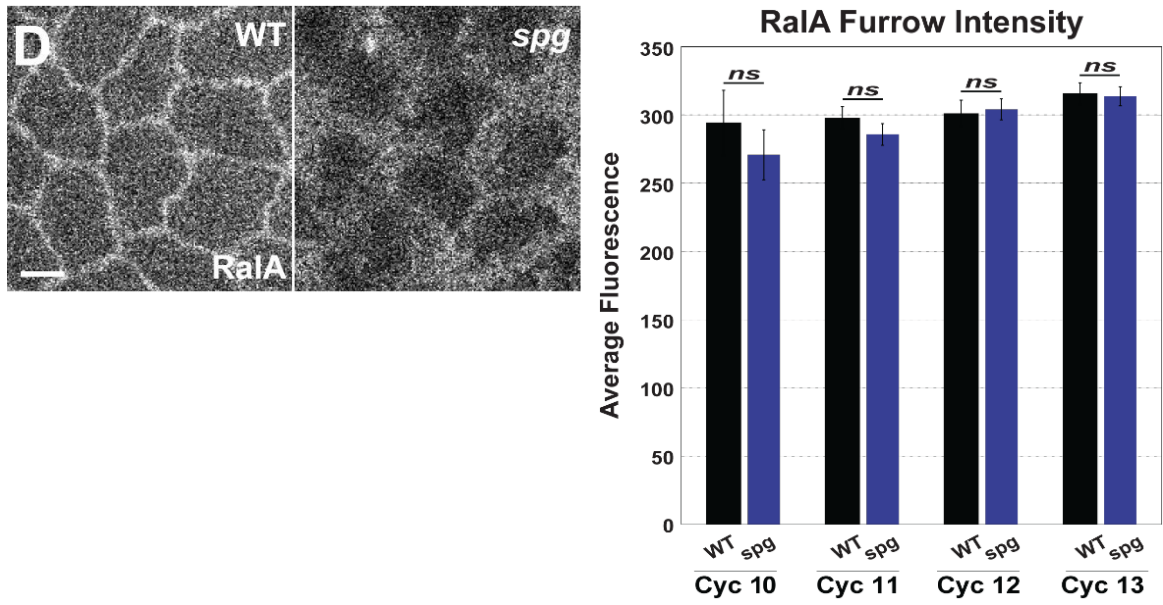
Figure 2 cont. Spg does not affect membrane trafficking pathways. (D) Still frames from live-imaging RalA at t=4 min in cycle 12 of wild-type and *spg* embryos (left). Average fluorescence intensity of RalA on furrows from cycle 10-13 in wild-type and *spg* embryos (right). Scale bar=5 µm.

sponge function is required for F-actin populations at furrows and apical caps

Next, we looked at the effects of _spg_ disruption on F-actin networks during furrow formation. Immunostaining for Spg in wild-type embryos revealed that Spg strongly co-localizes with F-actin on the furrows (Fig. 3A). When _spg_ is disrupted using shRNA, some F-actin is still localized on the membranes, but at significantly decreased levels as indicated by fluorescence intensity of the actin-binding domain of Moesin (MoeABD) (Fig. 3B). In cycles 10-13, fluorescence in wild-type furrows is up to 4.1X brighter than in _spg_ disrupted furrows (Fig. 3C).

Immunostaining additionally showed that Spg is present on apical actin caps (Fig. 3D). In wild-type embryos, apical F-actin forms a dome-shaped cap above each nucleus averaging at an area of approximately 216 μm^2 in cycle 10 and becoming smaller with each subsequent cycle as nuclei become more dense (Fig. 3F, left). When _spg_ is disrupted, however, apical F-actin is severely reduced, forming small cap-like structures above nuclei with an average area of 70 μm^2 in cycle 10, 67.4% smaller than in wild-type. With each consecutive cycle, these structures become smaller, averaging 34 μm^2 in cycle 13 compared to wild-type's 72 μm^2 caps (Fig. 3F, left). F-actin within these cap-like structures is also strongly reduced relative to their size; average intensity of MoeABD on caps in _spg_ disrupted embryos is 3.3-4.6X lower than wild-type caps in cycles 10-13 (Fig. 3E, F, right). Together, these data show that F-actin intensity and localization is strongly diminished on _spg_ disrupted syncytial caps and furrows, and suggests Spg may function in cytoskeletal remodeling pathways.
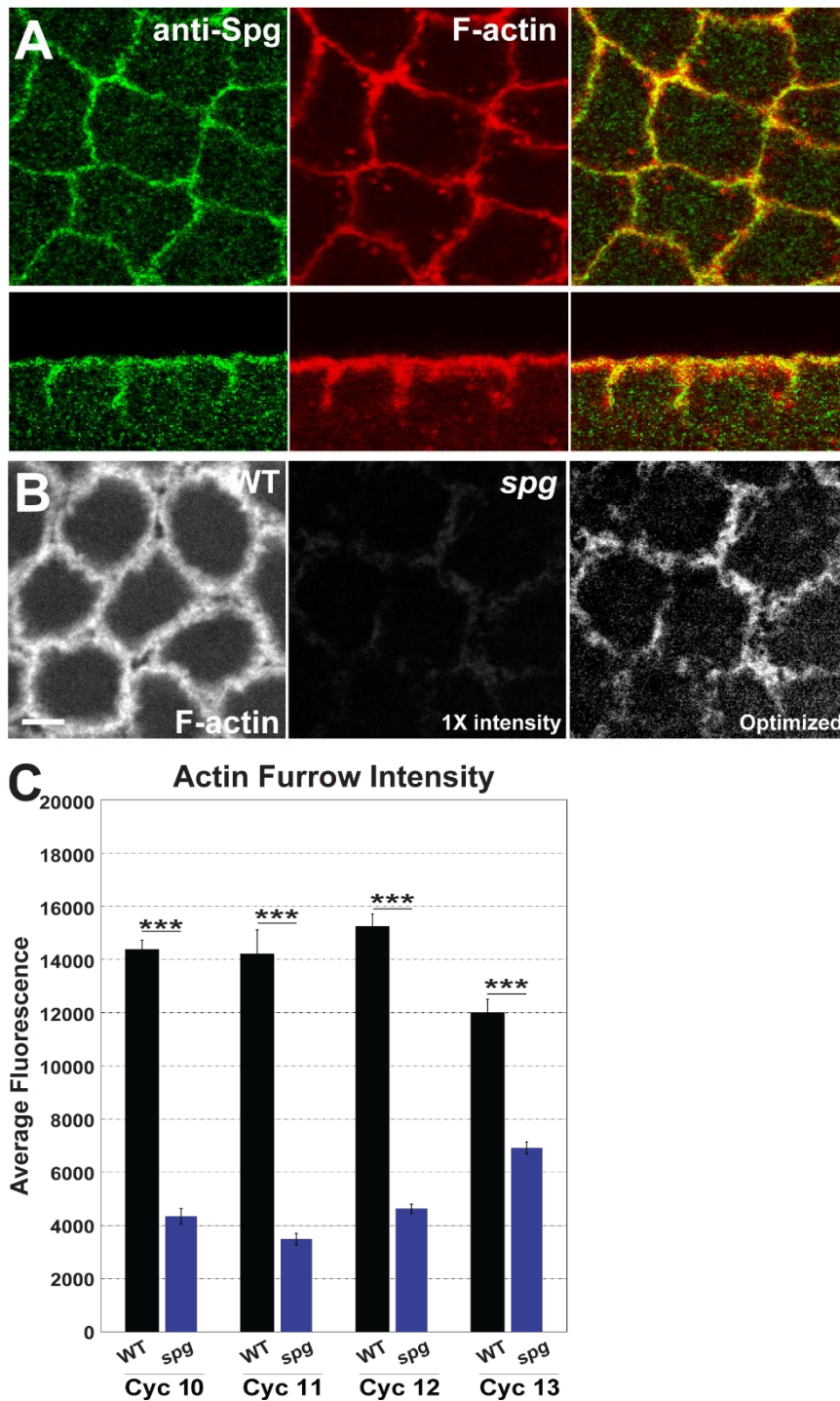
Figure 3. F-actin levels are reduced in *spg* embryos. (A) Immunostaining for Spg (green) and F-actin (Phalloidin; red) during syncytial cycle 12 shows top-down and side views of furrows. (B) Still images from live-imaging MoeABD (actin marker) at t=4 min in cycle 12 of wild-type and *spg* embryos. Scale bar=5 µm. (C) Average fluorescence intensity of MoeABD on furrows from cycle 10-13 in wild-type and *spg* embryos.
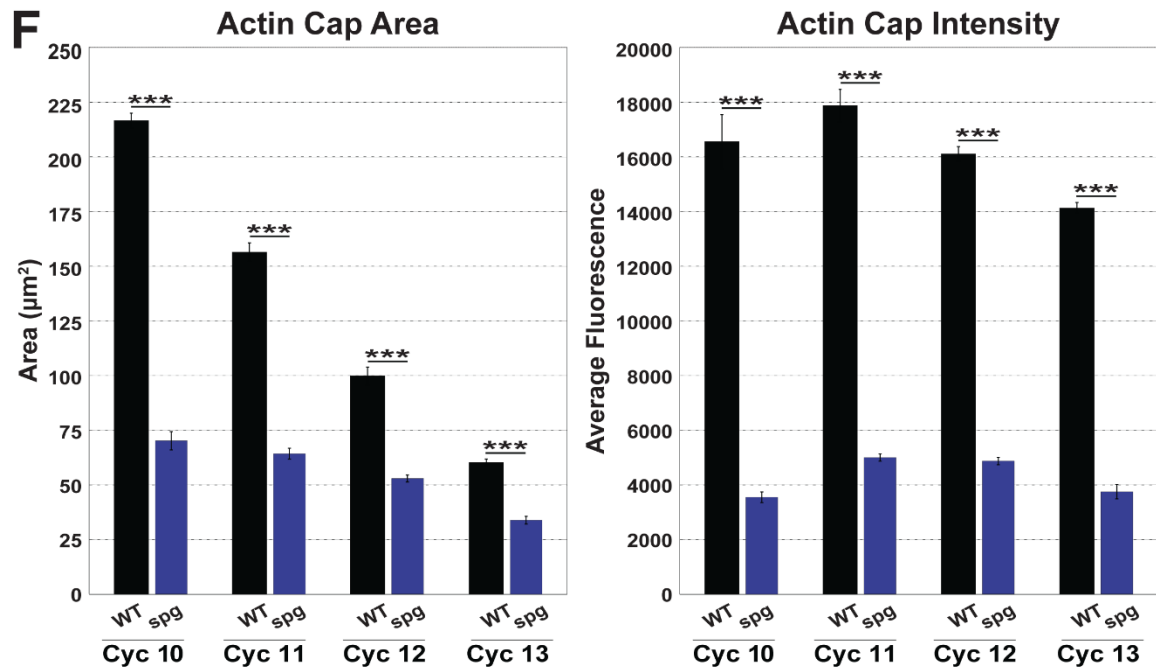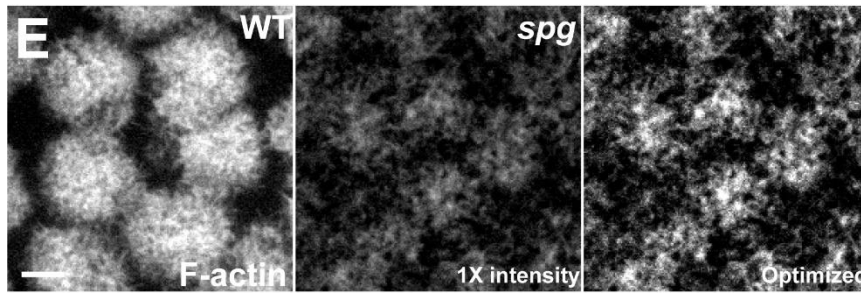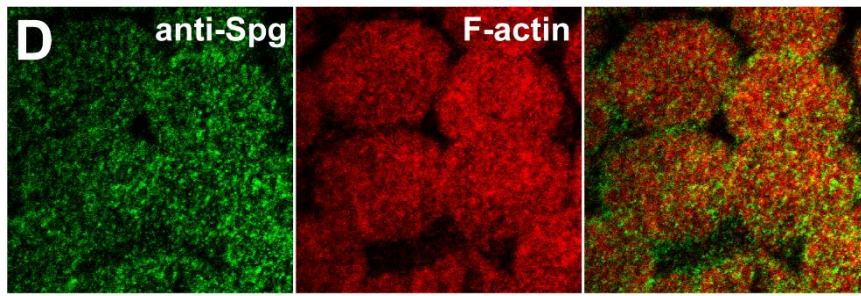
Figure 3 cont. F-actin levels are reduced in *spg* embryos. (D) Immunostaining for Spg (green) and F-actin (Phalloidin; red) during syncytial cycle 12 shows apical caps. (E) Still images from live-imaging MoeABD (actin marker) at t=2 min in cycle 12 of wild-type and *spg* embryos. Scale bar=5 µm. (F) Average area and fluorescence intensity of MoeABD on apical caps from cycle 10-13 in wild-type and *spg* embryos.

Sponge indirectly affects Diaphanous-mediated F-actin networks

Two populations of F-actin are involved in syncytial stages: Formins regulated linear F-actin found primarily in furrows, and Arp2/3 mediated branched F-actin found primarily in apical caps. To determine whether Spg is required for one or both of these populations, we first tested the effect of *spg* disruption on linear actin networks through measurements of the *Drosophila* formin Diaphanous (Dia). In the *dia* shRNA background, syncytial furrows form but are severely shortened (Fig. 4A-C). Comparable to wild-type and *spg* furrows, *dia* furrows follow typical ingression dynamics with measurable Ingression I, Stabilization, and Ingression II phases (Fig. 4B-D), but furrows only reach a maximum depth of 3.5 µm by cycle 13 (Fig. 5B-C). Compared to *spg* disrupted embryos (maximum furrow depth of 2.1 µm), *dia* disrupted embryos can build slightly longer furrows. These differences in furrow length suggest Spg may not be acting directly through the Dia pathway; however, these results indicate that Dia mediated linear actin networks are also needed to build furrows longer than 2-3 µm. Further evidence of this is seen when comparing Dia localization in a *spg* disrupted background. Immunostaining for anti-Dia showed that Dia does localize to the short, broad furrows produced in *spg* embryos, although mean fluorescence intensity is decreased nearly two-fold (Fig. 4E). Similarly, we compared anti-Spg immunostains in *dia* embryos to wild-type. In both backgrounds, Spg successfully co-localizes with F-actin on the furrows (Fig. 4F). This suggests that Dia is not necessary for Spg function, and further implies Spg may not be directly involved with Dia.

Lastly, if Spg acts in a distinct mechanism from that of Dia-mediated F-actin polymerization, it would be expected that knocking down both *spg* and *dia* would

26

produce an even stronger phenotype than either disruption alone. Indeed, when comparing furrows in *spg* shRNA, *dia* shRNA, and *dia;spg* double shRNA embryos, F-actin appears the most punctate and diffuse in *dia;spg* embryos. F-actin levels indicated by intensity of Phalloidin staining further reveals that *dia;spg* embryos possess the most severe reduction in F-actin levels (Fig. 4G). In all, these data suggest that branched actin networks produced in a Spg dependent pathway may be important for Dia to localize and nucleate linear actin networks along ingressing furrows.
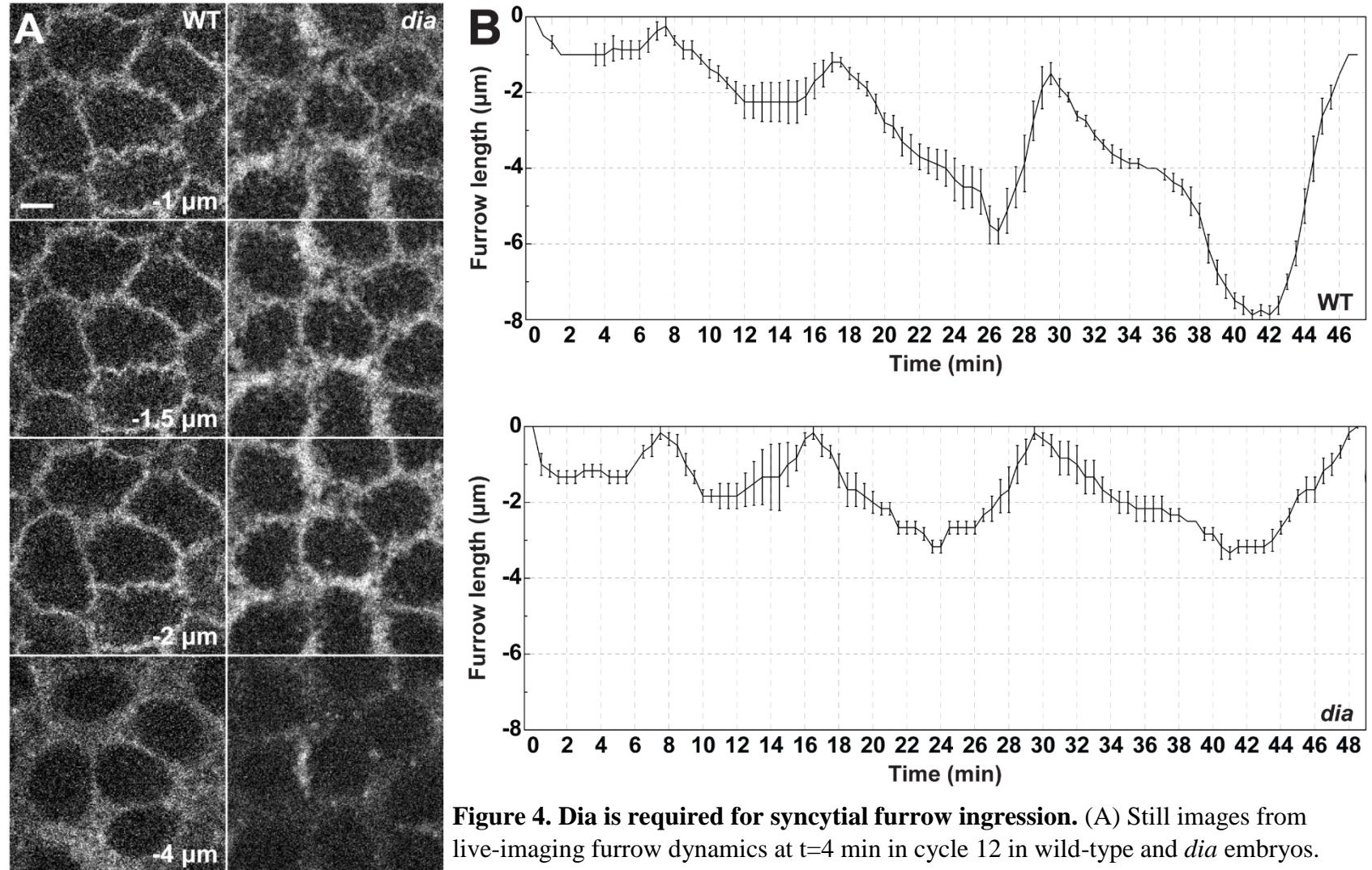
Figure 4. Dia is required for syncytial furrow ingression. (A) Still images from live-imaging furrow dynamics at t=4 min in cycle 12 in wild-type and *dia* embryos. Scale bar=5 µm. (B) Biphasic furrow ingression dynamics in wild-type and *dia* embryos from cycle 10-13.
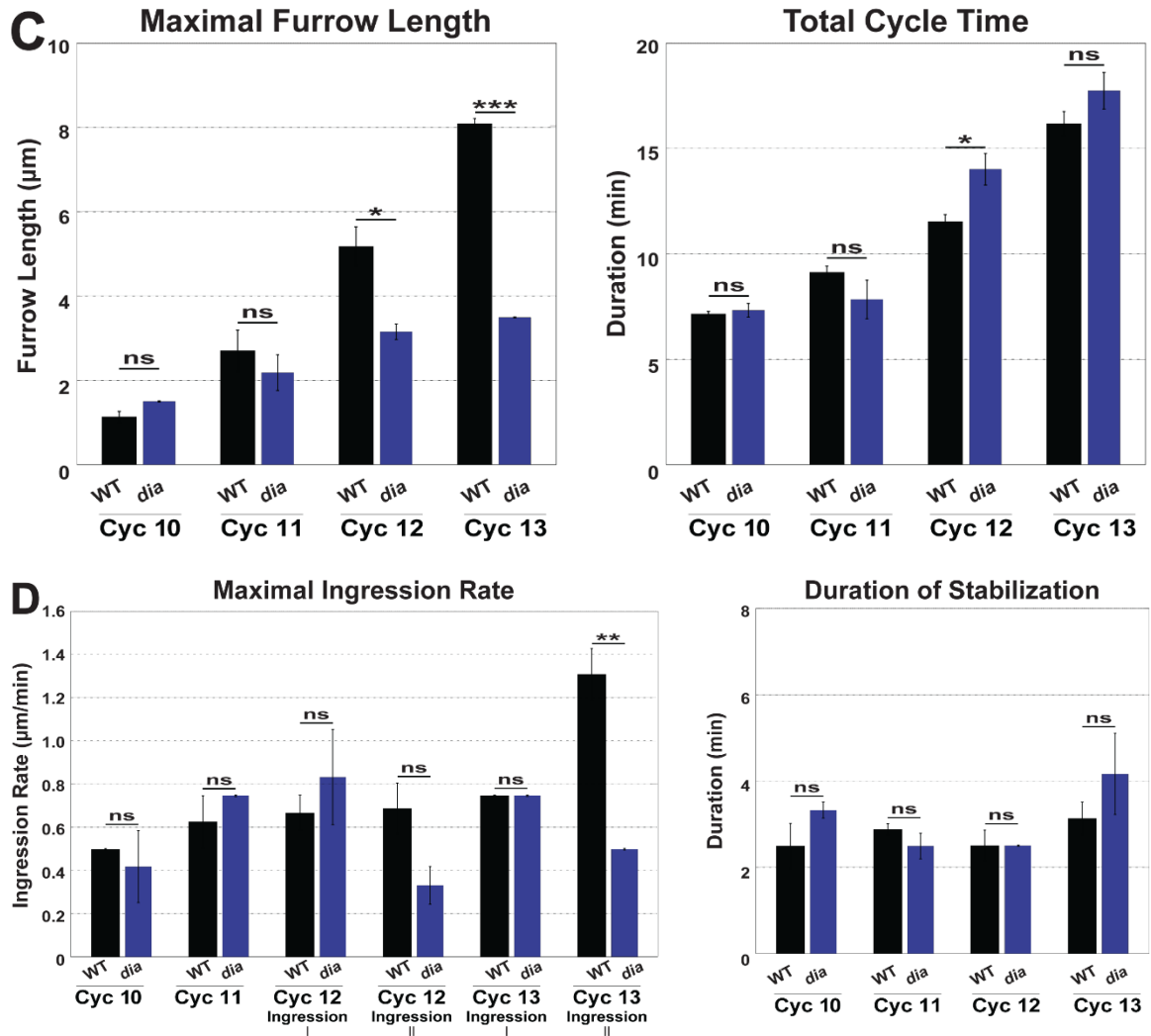
C Maximal Furrow Length

Total Cycle Time

D Maximal Ingression Rate

Duration of Stabilization

Figure 4 cont. Dia is required for syncytial furrow ingression. (C) Maximal furrow length and total cycle time from cycle 10-13 in wild-type and *dia* embryos. (D) Maximal ingression rate from cycle 10-13 Ingression I and Ingression II in wild-type and *dia* embryos, calculated from a 2-minute rolling window (left). Right shows duration of the Stabilization phase of each cycle 10-13 in wild-type and *dia* embryos.
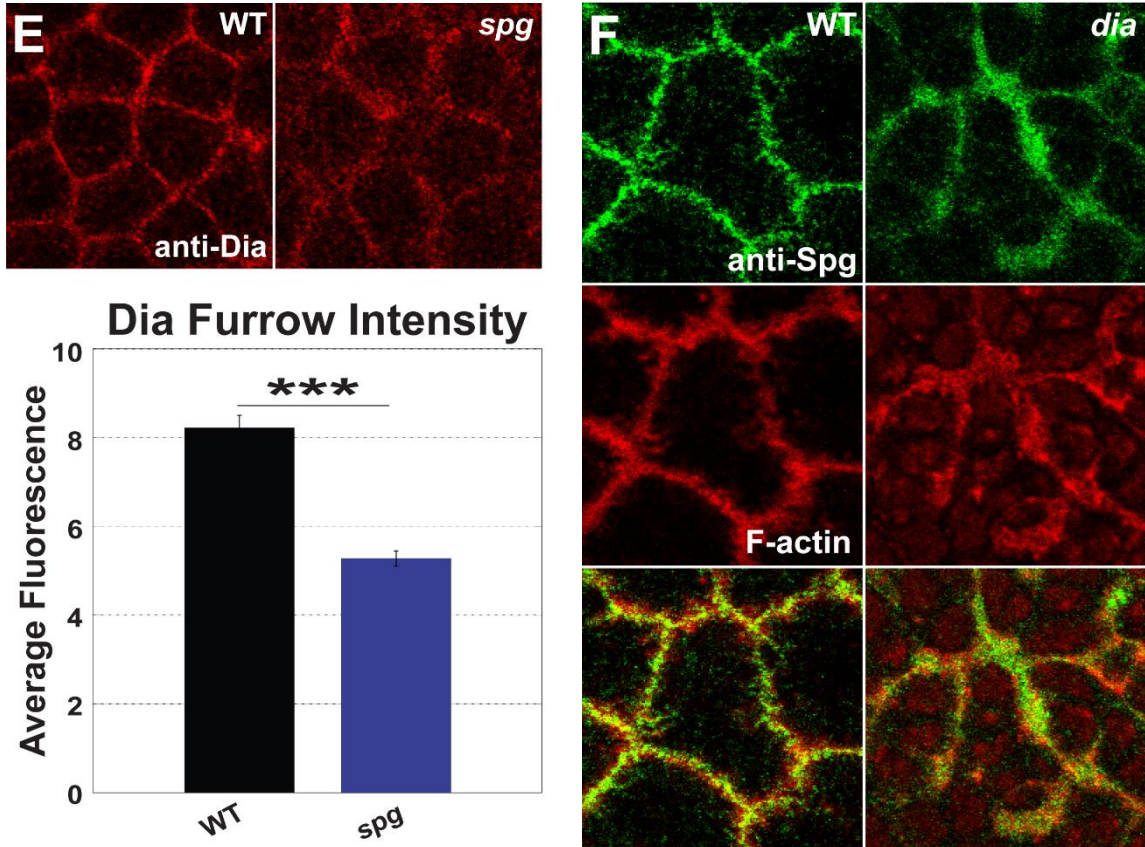
Figure 4 cont. Dia is required for syncytial furrow ingression. (E) Immunostaining for Dia in wild-type and *spg* embryos shows top-down view of furrows (top). Dia fluorescence intensity from cycle 10-14 is quantified in wild-type and *spg* embryos (bottom). (F) Immunostaining for Spg (green) and F-actin (Phalloidin; red) in wild-type and *dia* embryos shows top-down view of furrows.
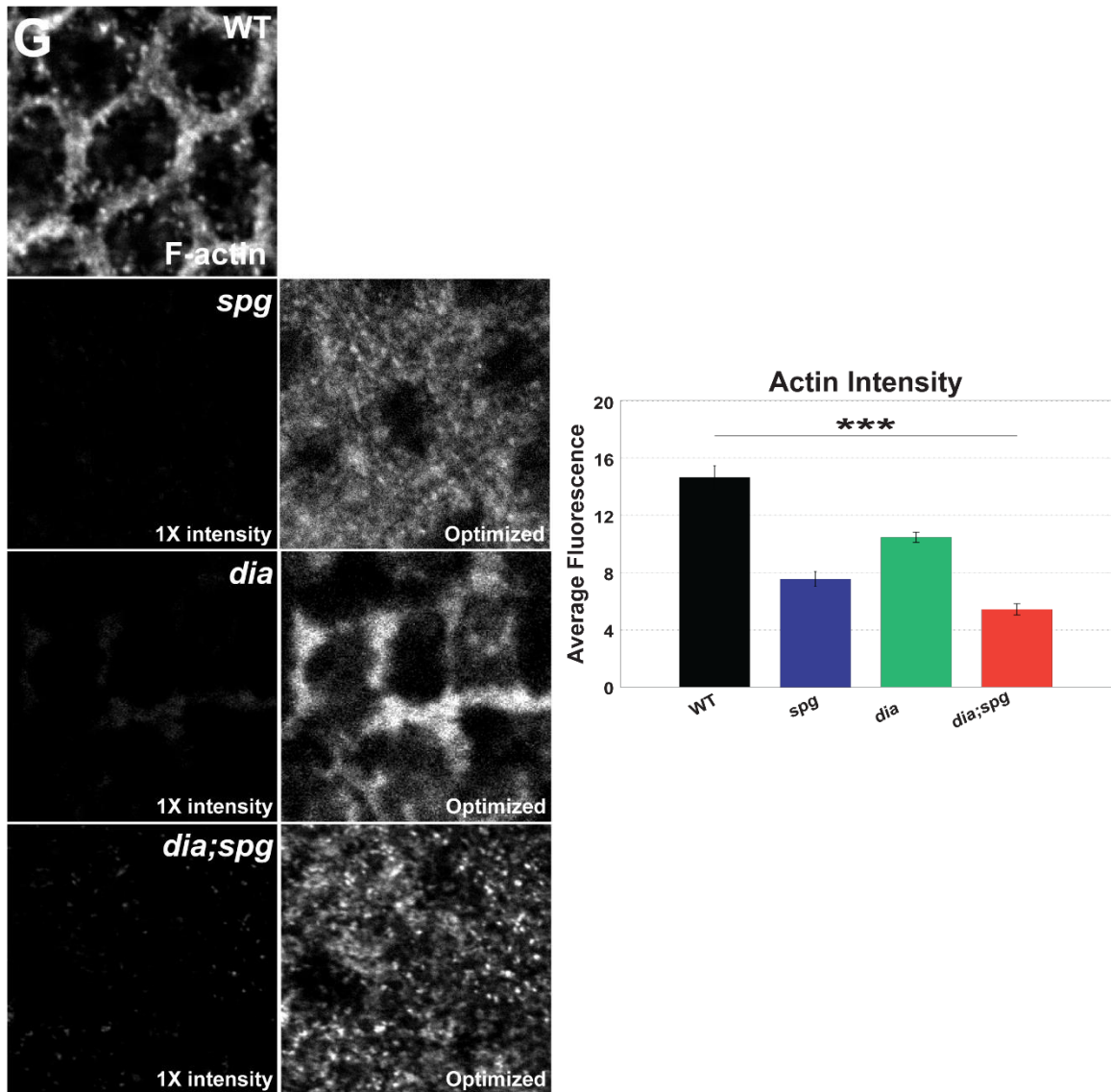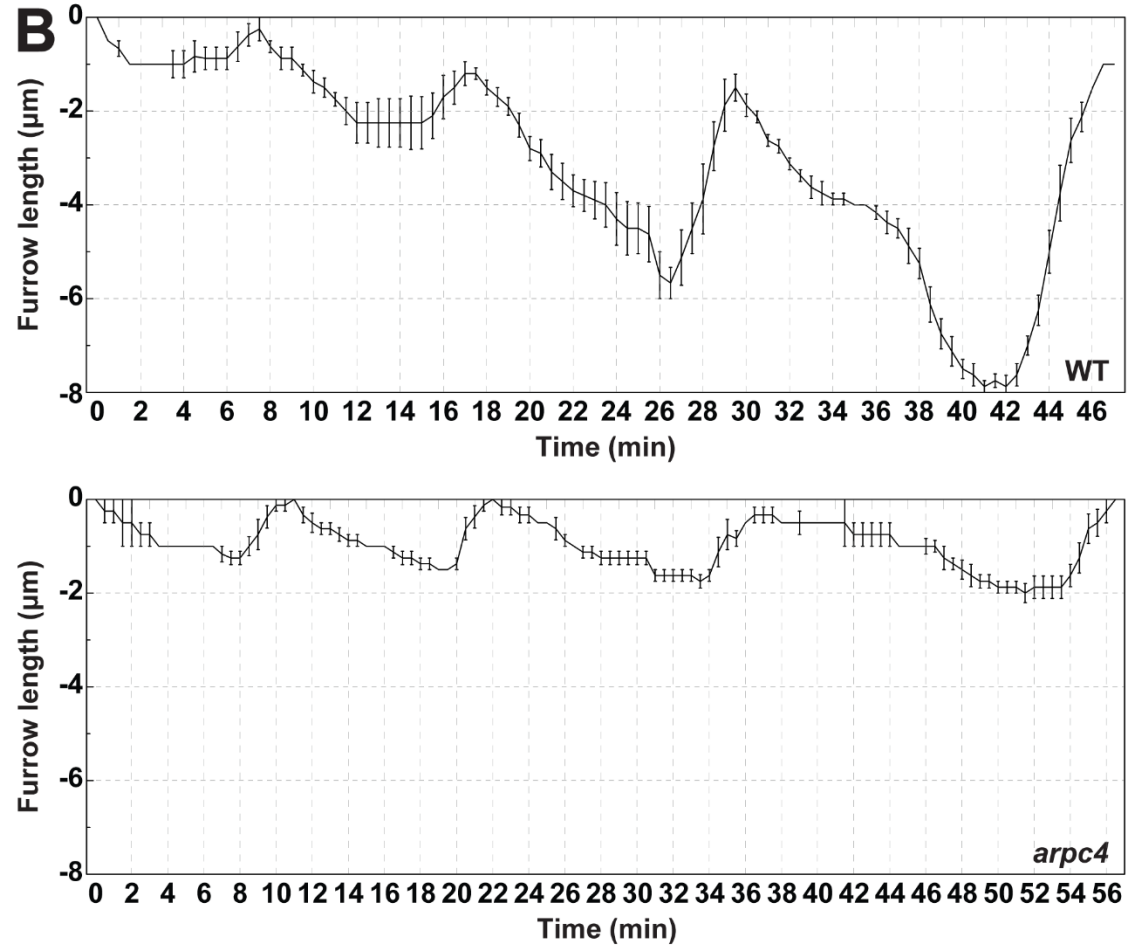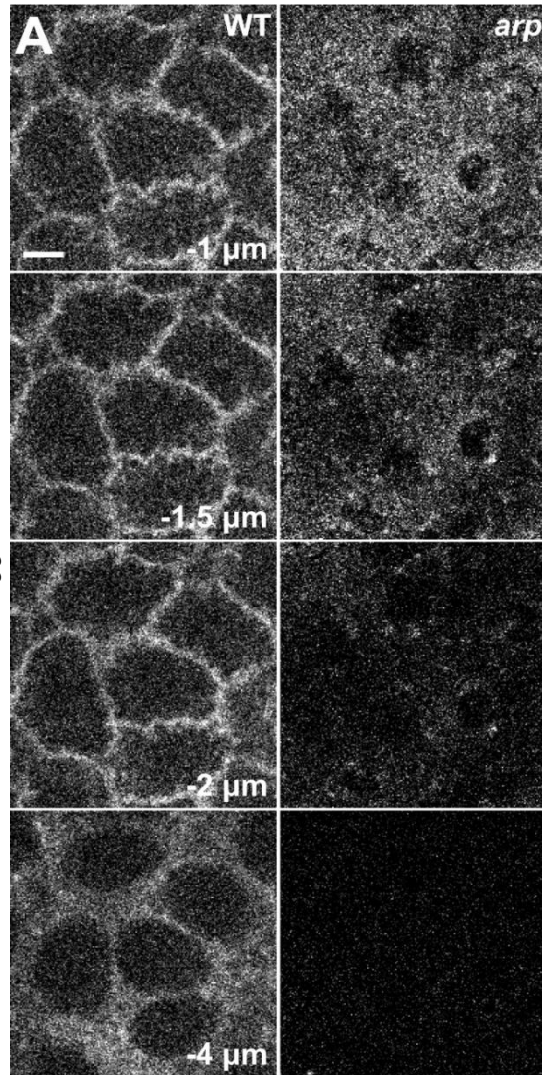
Figure 4 cont. Dia is required for syncytial furrow ingression. (G) Immunostaining for F-actin (Phalloidin) in wild-type, *spg*, *dia*, and *dia;spg* double shRNA embryos. Average intensity from cycles 10-14 is quantified (right).

**Sponge is required for Arp2-3 mediated actin polymerization**

We next tested the involvement of Spg in the Arp2/3 mediated branched actin networks prominent in apical caps. We first observed syncytial phenotypes in an *arpc4* shRNA background. These embryos produce severely shortened furrows, reaching a maximum length of 2.1 µm by cycle 13 (Fig. 5A-C). These furrows are built in the typical biphasic manner with a measurable stabilization phase in each cycle, but with slightly slower ingression rates than wild-type (Fig. 5D). Interestingly, maximal ingression rates in each ingression phase of *spg* and *arpc4* embryos are equal from cycle 11-cycle 13 Ingression I (Fig. 1E, 5D).

The Arp2/3 subunit Arpc1GFP was then observed in wild-type and *spg* embryos. In wild-type embryos, Arpc1GFP localizes strongly to the actin caps during syncytial cycles (Fig. 5E, left). Strikingly, in *spg* embryos, this localization is entirely lost as Arpc1 appears as dispersed puncta throughout the cytoplasm—puncta that are not observed in wild-type embryos (Fig. 5E, right). Overall fluorescence intensity further indicates that there is significantly less localized Arpc1 in *spg* embryos, as intensity within areas comparable to cap areas in wild-type embryos is reduced 95% by cycle 13 (Fig. 5F). The similar phenotype between *spg* and *arpc4* embryos, along with the drastic mislocalization of Arpc1 in a *spg* background suggest that Spg is strongly involved in an Arp2/3 mediated pathway of F-actin polymerization.

Figure 5. Arp2/3 is required for syncytial furrow ingression. (A) Still images from live-imaging furrow dynamics at t=4 min in cycle 12 in wild-type and *arpc4* embryos. (B) Biphasic furrow ingression dynamics in wild-type and *arpc4* embryos from cycle 10-13.
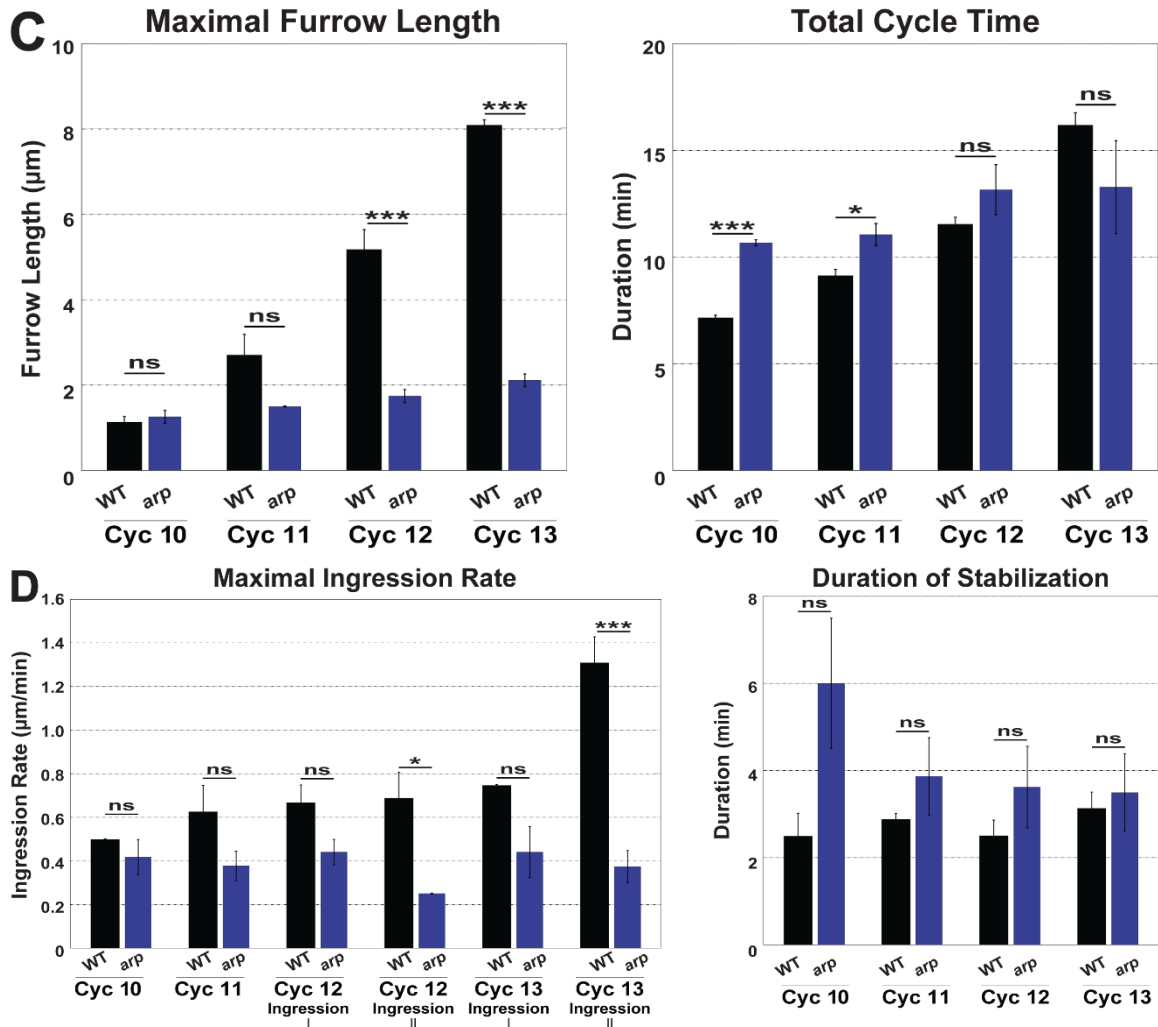
Figure 5 cont. Arp2/3 is required for syncytial furrow ingression. (C) Maximal furrow length and total cycle time from cycle 10-13 in wild-type and *arpc4* embryos. (D) Maximal ingression rate from cycle 10-13 Ingression I and Ingression II in wild-type and *arpc4* embryos, calculated from a 2-minute rolling window (left). Right shows duration of the Stabilization phase of each cycle 10-13 in wild-type and *arpc4* embryos.
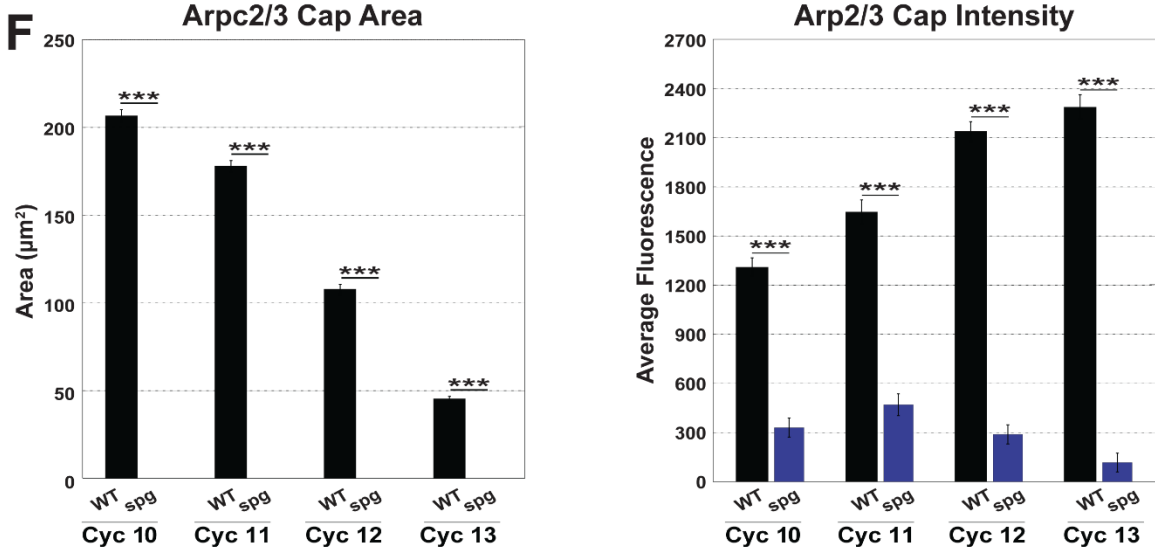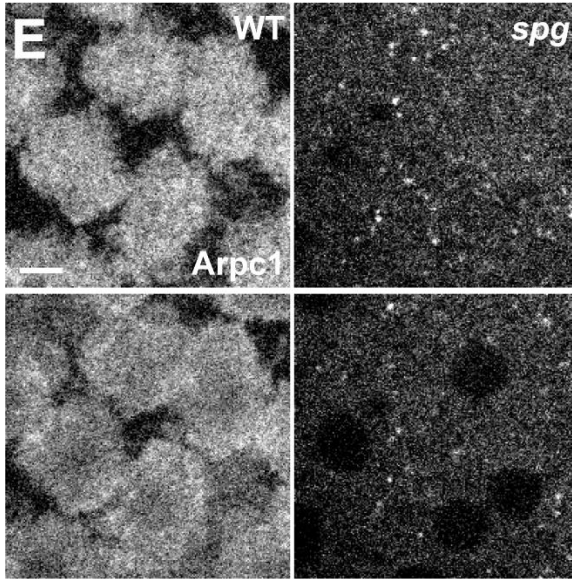
Figure 5 cont. Arp2/3 is required for syncytial furrow ingression. (E) Still images from live-imaging Arpc1GFP at t=2 min in cycle 12 of wild-type and *spg* embryos. Scale bar=5 µm. (F) Average apical cap size (left) and fluorescence intensity of Arpc1 on apical caps or comparable apical areas (right) from cycle 10-13 in wild-type and *spg* embryos.

Arp2/3 Disruption Resembles *spg*

To further compare the similar phenotypes seen in *spg*, *dia*, and *arpc4* embryos, we more carefully looked at furrow morphology and F-actin localization to the apical cap. During biphasic furrow ingression, wild-type furrows become progressively thinner from cycles 10-13, and additionally undergo a transition from broad furrows during the Ingression I phase of each cycle to sharper furrows during Ingression II (Fig. 6A). *spg* furrows, however, appear as broader, less distinct furrow structures throughout each cycle (Fig. 6A). Although still maintaining the pattern of becoming thinner as nuclear density increases, as well as in the transition from Ingression I to II, *spg* furrows are significantly wider in every syncytial ingression phase than their wild-type counterparts (Fig. 6B). In contrast, *dia* furrows are very sharp and defined (Fig. 6A). The width of these furrows in early cycles (10-11) is even thinner than those in wild-type, and not significantly different from wild-type during Ingression I of cycles 12-13 (Fig. 6B). Interestingly, *dia* furrows are only significantly broader than wild-type during Ingression II phases, suggesting Dia may be especially important during these periods of rapid furrow growth. Measurements of furrow width in *arpc4* embryos indicated furrows are significantly wider than wild-type in every ingression phase, comparable to the width of *spg* furrows (Fig. 6B).

Similarly, apical caps more closely phenocopied *spg* cap-like structures in *arpc4* embryos than in *dia* embryos (Fig. 6C). Cap area in *dia* embryos is smaller than in wild-type, but significantly larger than in *spg* embryos (Fig. 6D). In addition, while intensity of Actin on these caps is reduced, it is not as severely reduced as in in *spg* (Fig. 6D). As caps are mainly comprised of branched F-actin, these results are not surprising and likely reflect previously reported roles of Dia in cap expansion (Cao et al., 2010). Apical caps in

arpc4 shRNA embryos also begin significantly larger than *spg* disrupted caps, but reduce very quickly in size and are 15-23% smaller than *spg* caps in cycles 12-13 (Fig. 6D). Intensity levels in *arpc4* caps are much more similar to those in *spg* cap, more likely reflecting a *spg*-like phenotype than a *dia*-like disruption (Fig. 6D).
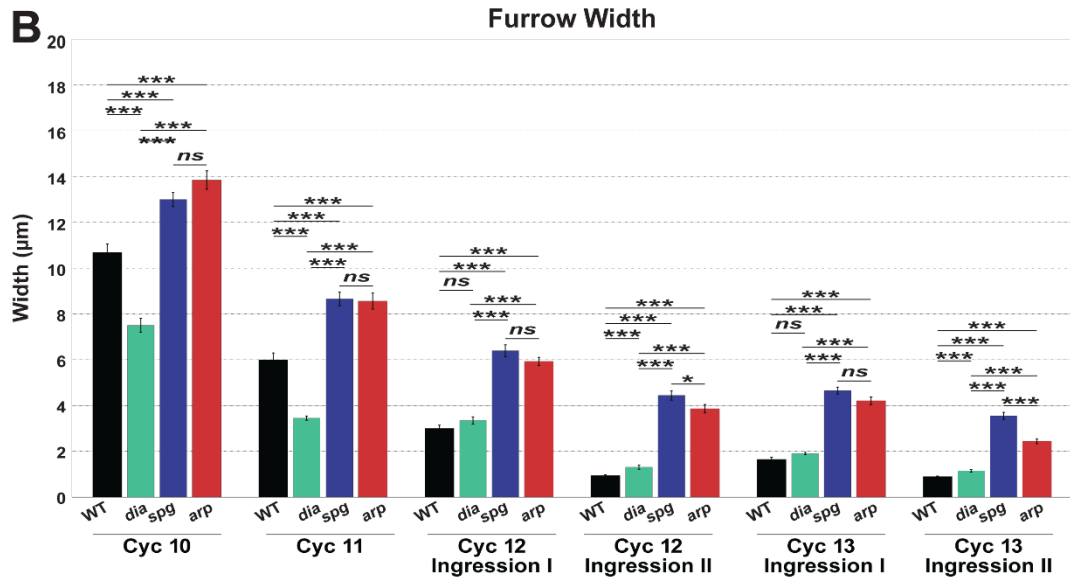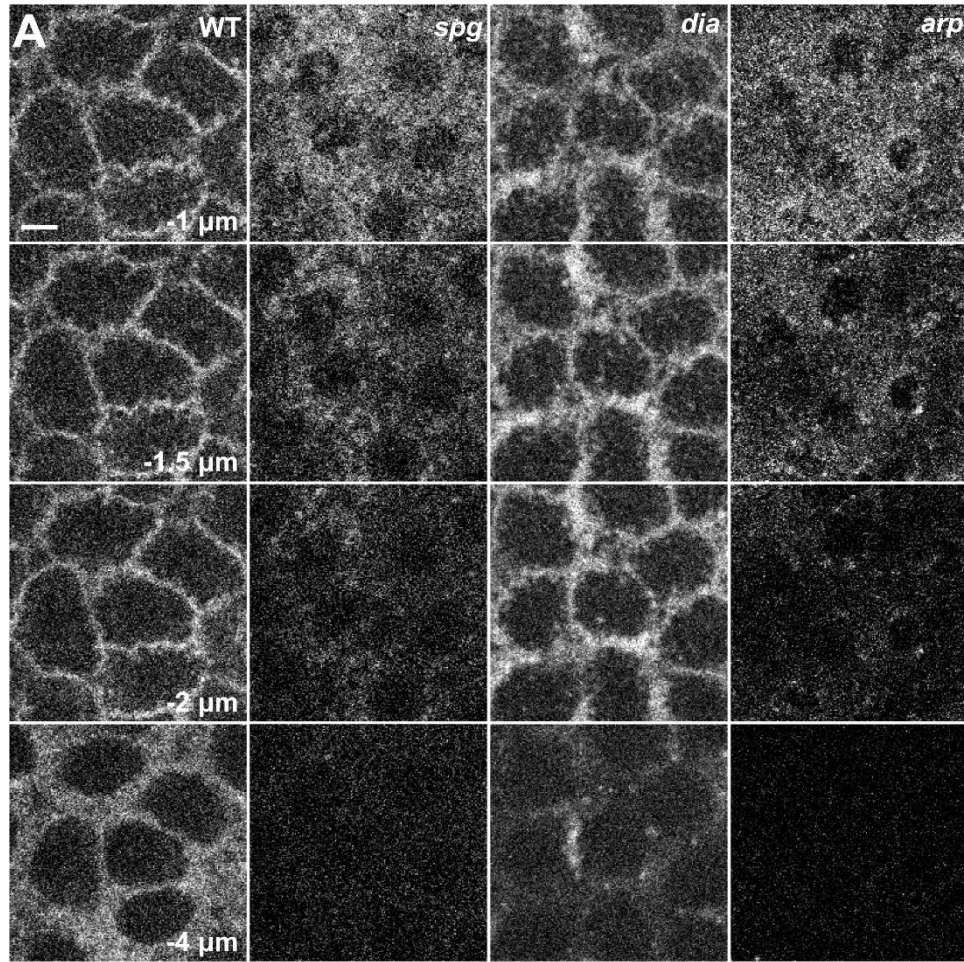
Figure 6. Comparison of syncytial phenotypes. (A) Still images from live-imaging furrow dynamics at t=4 min in cycle 12. Scale bar=5 µm. (B) Average furrow widths measured at representative time points in each ingression phase (see methods).
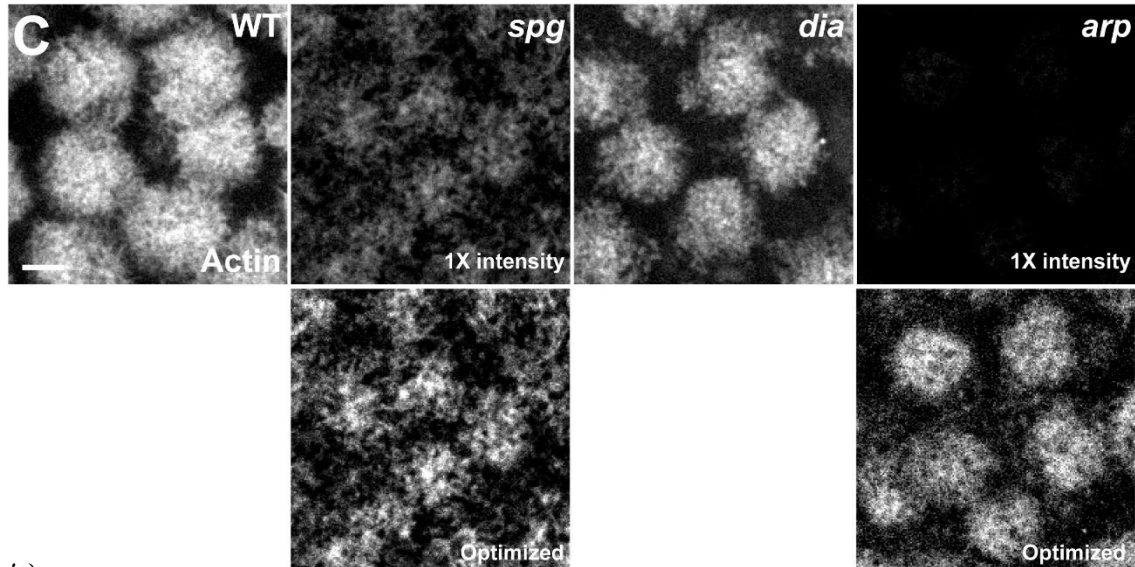
Figure 6. Comparison of syncytial phenotypes, cont. (C) Still images from live-imaging MoeABD (actin marker) at t=2 min in cycle 12. Scale bar=5 µm. (D) Average area and fluorescence intensity of MoeABD on apical caps from cycle 10-13.

39
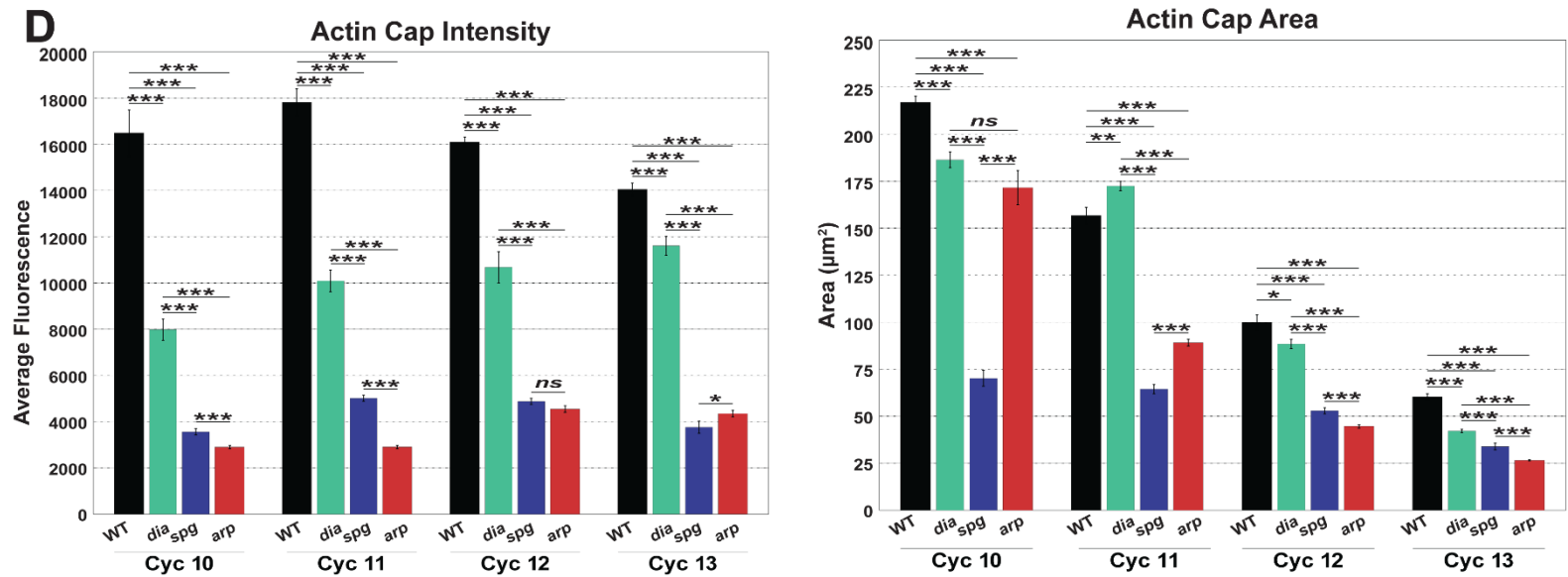
Spg is required for Arp2/3 regulator localization to the cap and apical furrow

To determine the upstream Arp2/3 regulators Spg may be acting through, we looked at localization of Cortactin, DPod1, Scar, and Coronin in a *spg* disrupted background. Consistently, these proteins are present on the actin caps in wild-type embryos, while also localizing increasingly to the apical-most portions of the furrows as the cycles progress (Fig. 4A-D, left). When Spg function is lost, localization of these proteins decreases at the apical cap. Interestingly, the intensity of each regulator, with the exception of Cortactin, was reduced as well (Fig. 4A-D). The localization to the apical furrows is completely lost for all of these proteins in the *spg* background, and instead dispersed puncta are seen (Fig. 4B-E). In summary, Arp2/3 and its regulators are severely mislocalized in Spg disrupted embryos, demonstrating that Spg is a critical factor required for recruiting these proteins to the apical caps and furrows to facilitate actin polymerization.
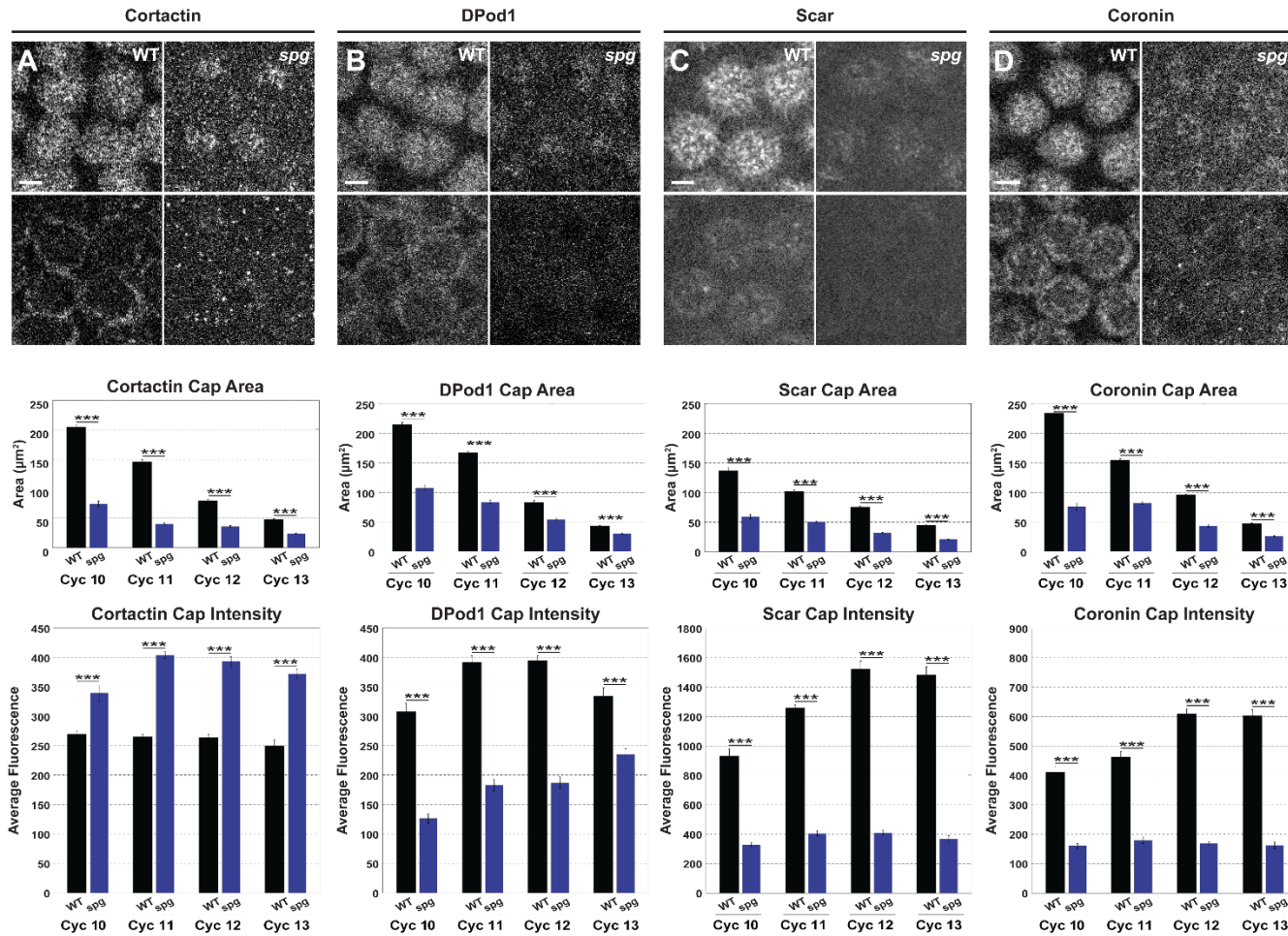
Figure 7. Spg is required for localization of Arp2/3 regulators to caps and apical furrows. Still images from live-imaging CortactinGFP (A), DPod1GFP (B), ScarGFP (C), and CoroninGFP (D) at t=2 minutes in cycle 12 of wild-type and *spg* embryos. Images show apical caps (top) and transition point between caps and furrows (bottom). Apical cap area and average intensity of each Arp2/3 regulator from cycle 10-13 of wild-type and *spg* embryos are quantified (bottom). Scale bar=5 µm.

Sponge is not required for recruitment of Rac1 or Rap1 in syncytial stages

As Spg has been previously implicated as a Rac1GEF (Morishita et al., 2014), we wanted to see how *rac1* shRNA affected furrow behaviors. In *rac1* embryos, furrow dynamics were very similar to those in wild-type embryos, with furrows reaching depths of about 8 µm by cycle 13 and ingressing at similar rates (Fig. 6A-D). Although furrows appeared largely unaffected, a nuclear fallout phenotype appeared to be a main effect of *rac1* disruption (data not shown). As this phenotype typically indicates a disruption to the actin cap, a structure strongly disrupted in *spg* embryos, we looked at actin localization on caps in *rac1* embryos. Area and intensity measurements of MoeABD on *rac1* caps are significantly lower than wild-type caps (Fig. 6E), although not as severely as in *spg* embryos (compare to Fig. 3F). However, given this similar phenotype, we next measured the localization of Rac1 in *spg* embryos. Imaging of Rac1GFP indicated that Rac1 does localize to the plasma membrane furrows as in wild-type, and at intensities not significantly different than in wild-type through cycle 12 (Fig. 6F). This localization, along with the lack of shortened furrow phenotype in *rac1* embryos, suggests that during this stage of development Spg does not act as a Rac1GEF.

Spg has also been shown to function as a Rap1GEF in several stages of *Drosophila* development (Biersmith et al., 2011; Biersmith et al., 2015; Eguchi et al., 2013). Initial scoring of *rap1* embryos revealed that while 72% of *spg* embryos show defects by cellularization, only 34% of *rap1* embryos have defects in this time frame (data not shown). To further test Rap1 function in syncytial stages, we looked at Rap1 localization in *spg* embryos. In wild-type embryos, Rap1 localizes to the plasma membrane furrows. When Spg is disrupted, Rap1 remains on the furrows at intensities

not significantly different or higher than those in wild-type embryos (Fig. 6G). This

indicates that Spg is likely not a Rap1GEF in syncytial stages.
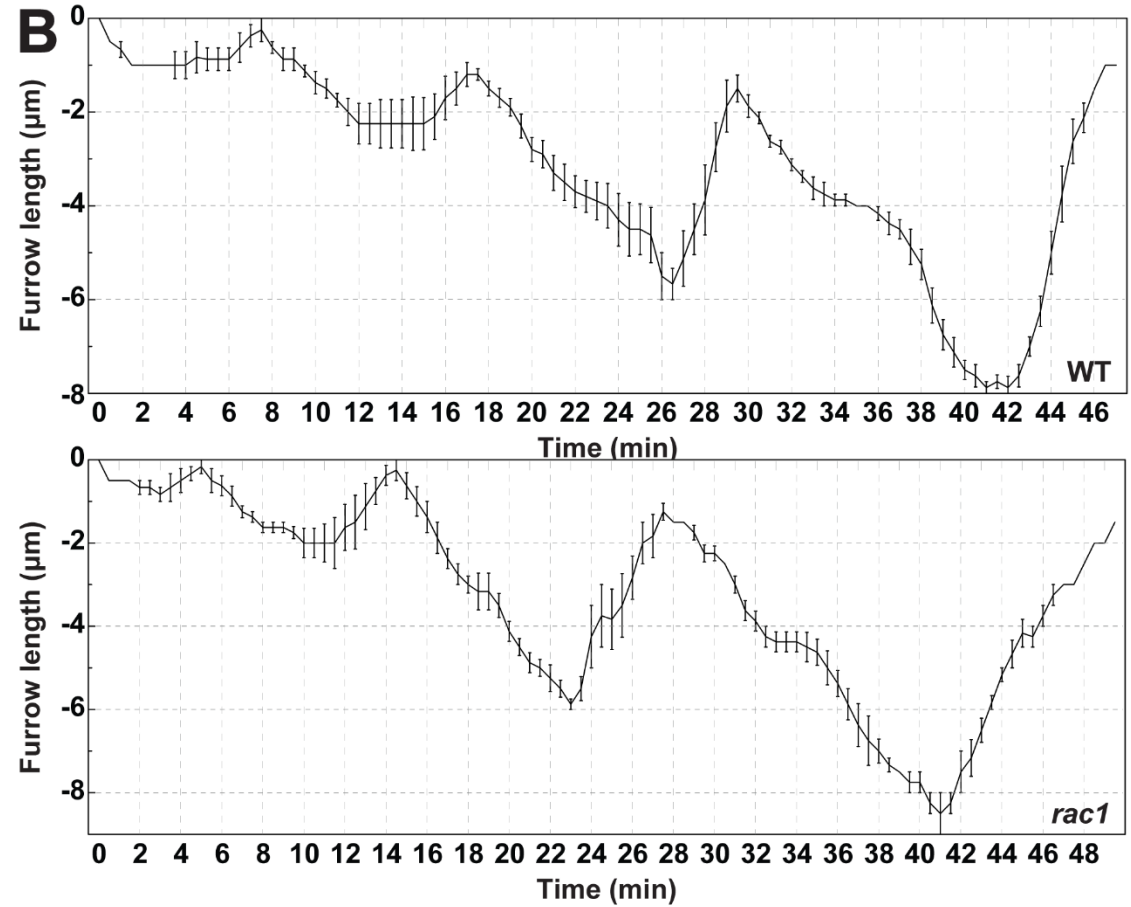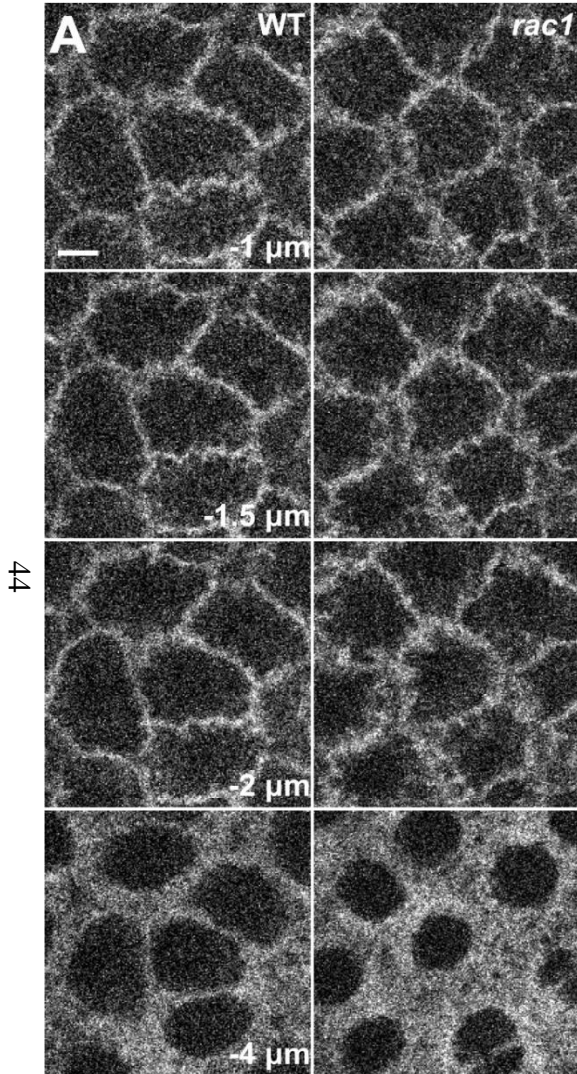
Figure 8. Spg does not act through Rac1 or Rap1. (A) Still images from live-imaging furrow dynamics at t=4 min in cycle 12 in wild-type and *rac1* embryos. Scale bar=5 µm. (B) Biphasic furrow ingression dynamics in wild-type and *rac1* embryos from cycle 10-13.
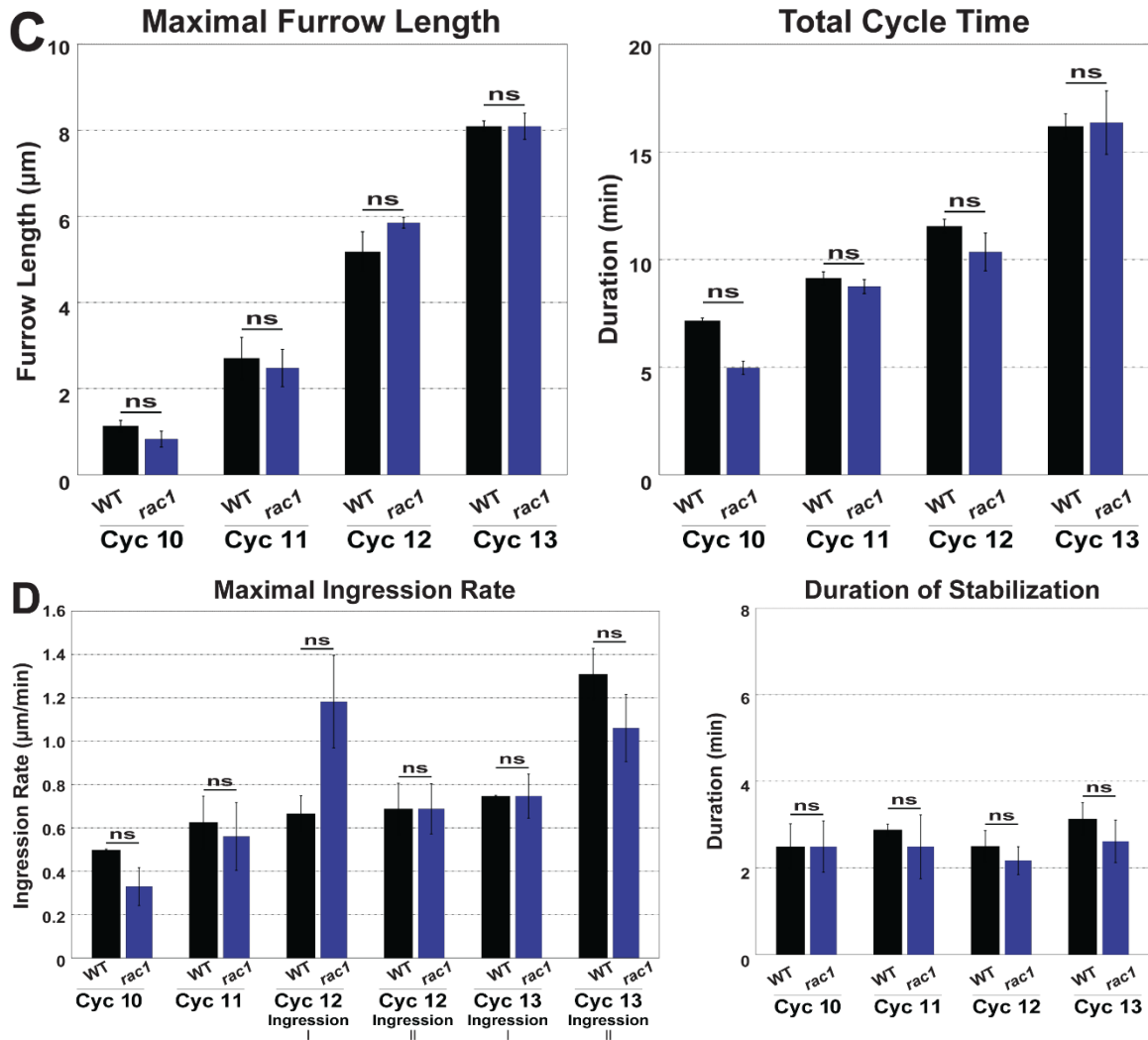
Figure 8 cont. Spg does not act through Rac1 or Rap1. (C) Maximal furrow length and total cycle time from cycle 10-13 in wild-type and *rac1* embryos. (D) Maximal ingression rate from cycle 10-13 Ingression I and Ingression II in wild-type and *rac1* embryos, calculated from a 2-minute rolling window (left). Right shows duration of the Stabilization phase of each cycle 10-13 in wild-type and *rac1* embryos.
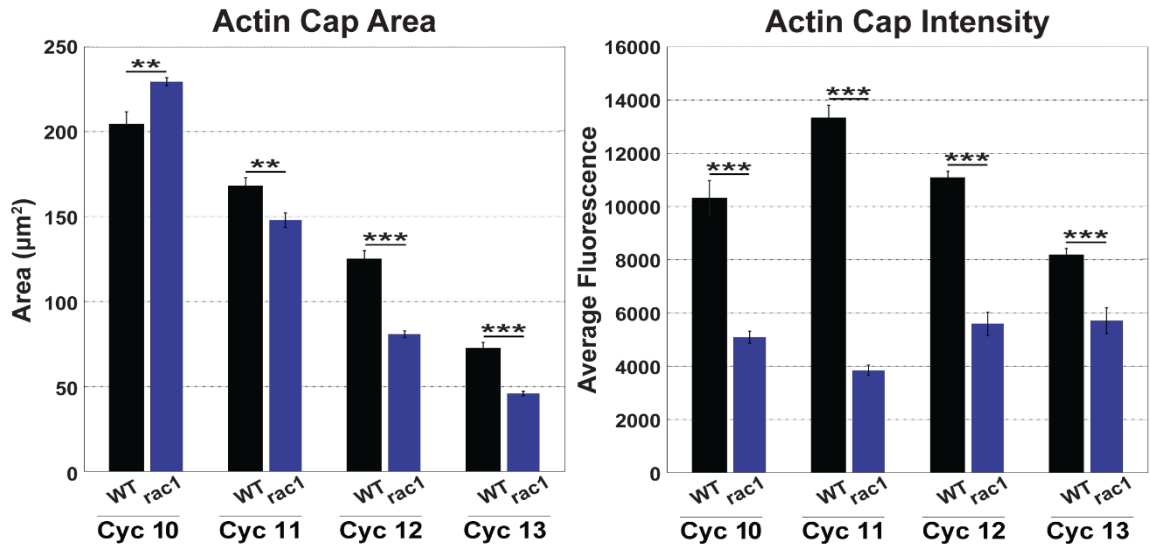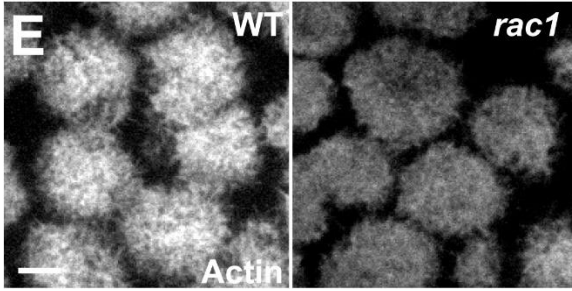
Figure 8 cont. Spg does not act through Rac1 or Rap1. (E) Still images from live-imaging MoeABD at t=2 min in cycle 12 of wild-type and *rac1* embryos. Average apical cap size (left) and fluorescence intensity of MoeABD on apical caps (right) from cycle 10-13 in wild-type and *rac1* embryos. Scale bar=5 µm.
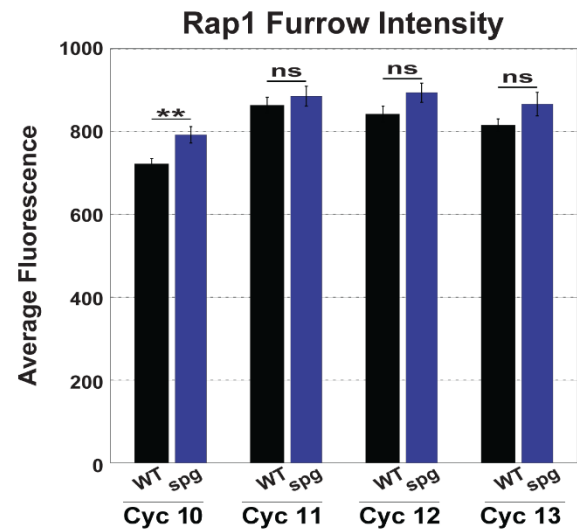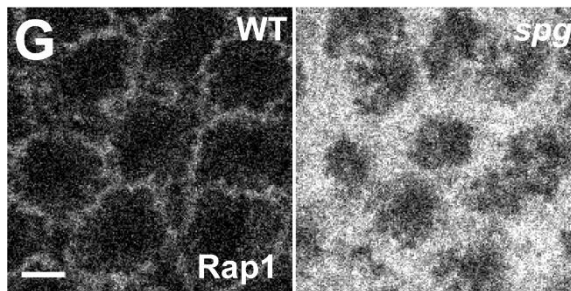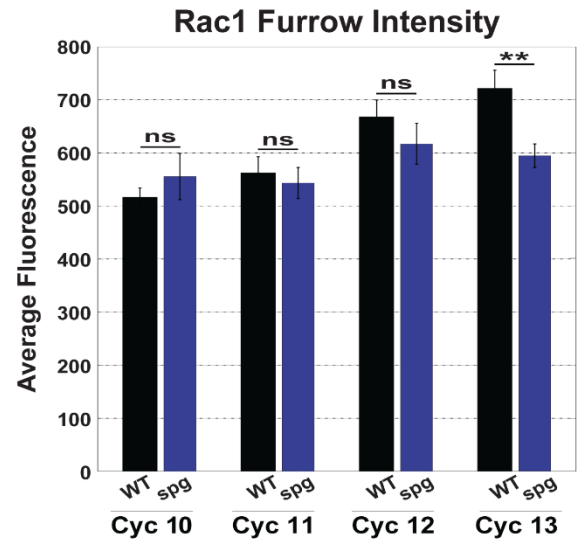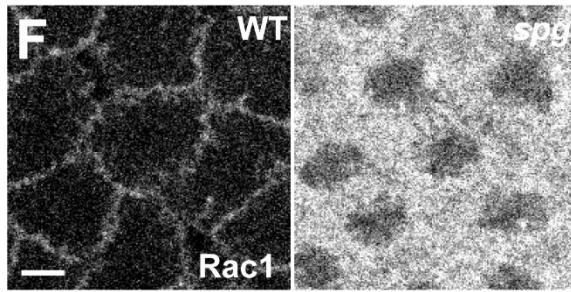
Figure 8 cont. Spg does not act through Rac1 or Rap1. (F) Still images from live-imaging Rac1GFP at t=4 min in cycle 12 of wild-type and *spg* embryos (left). Average fluorescence intensity of Rac1 on furrows from cycle 10-13 in wild-type and *spg* embryos is quantified (right). (G) Still images from live-imaging Rap1 at t=4 min in cycle 12 of wild-type and *spg* embryos (left). Average fluorescence intensity of Rap1 on furrows from cycle 10-13 in wild-type and *spg* embryos is quantified (right). Scale bar=5 µm.

Discussion

Overall Conclusions

This work has revealed that Spg is critically required for the organization of Arp2/3-mediated F-actin in the syncytial *Drosophila* blastoderm. *spg* knockdown causes mislocalization and decreased levels of Arp2/3 subunits and Arp regulators such as Cortactin, DPod1, Coronin, and Scar (Fig. 5, 7). Interestingly, Spg regulation of F-actin is essential for the transition of these regulators from caps onto apical regions of the growing furrows, as Cortactin, DPod1, Coronin, and Scar are absent on ingressing furrows in *spg* knockdown embryos (Fig. 7). This leads to inadequate branched actin networks resulting in short furrows, no longer than 2.1 µm in length through cycle 13, and small residual cap-like structures, as small as 33% the wild-type cap area (Fig. 1, 3). Based on this, we propose a mechanism in which Spg regulates and recruits Scar, Coronin, DPod1, and Cortactin to the apical caps, and these proteins in turn recruit and activate Arp2/3 activity. As the new Actin cap forms and expands, Arp2/3 and regulators remain associated with the branched Actin network and are present on the ring-like structure at the transition point from cap to furrow. This is necessary for proper linear F-actin nucleation and polymerization by Diaphanous to build sufficiently long furrows in each cycle (Fig. 9).
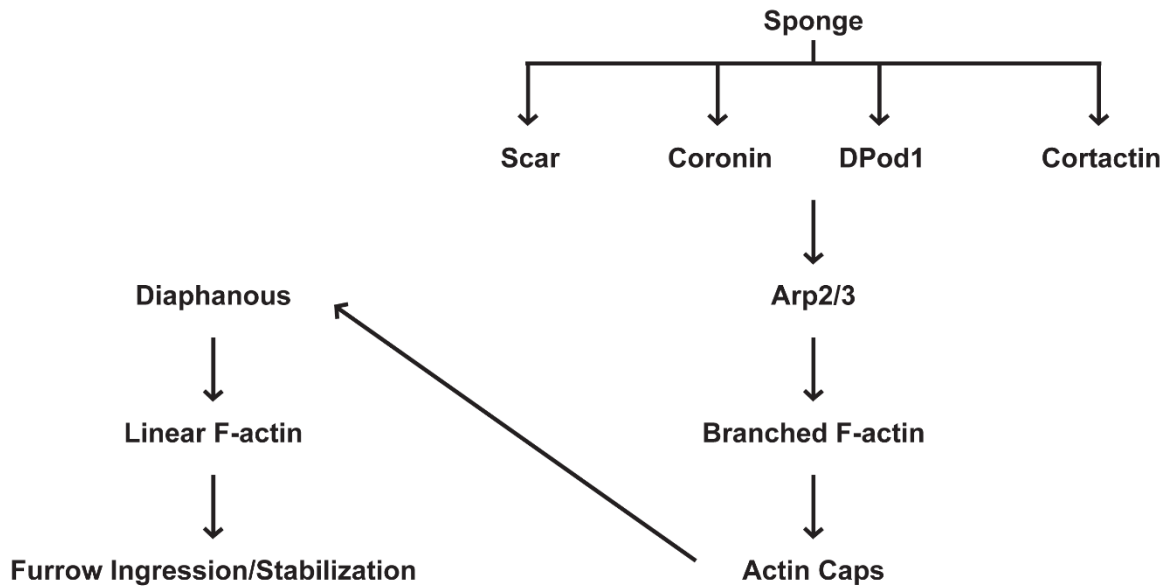
Figure 9. Proposed model of Spg activity in syncytial embryos. Data suggests that Spg is a master-regulator of Scar, Coronin, DPod1, and Cortactin in syncytial stages of *Drosophila* embryos. These proteins in turn regulate Arp2/3 localization to apical regions allowing branched F-actin networks to form apical caps above nuclei. These cap structures are necessary for Diaphanous-mediated linear F-actin networks to support increasingly long furrows to adequately separate dividing nuclei.

Spg as a master regulator of furrow ingression

Successful cell division relies on furrows physically separating neighboring nuclei. As these nuclei divide and become more densely packed, the risk of chromosomal missegregation or mitotic collapse rises if furrows do not adequately segregate neighboring nuclei or provide appropriate anchoring points for spindles. It has previously been shown that furrow length is negatively correlated with mitotic defects (Xie and Blankenship, 2018); in *spg* embryos, where furrows do not ingress past ~2 µm, severe missegregation beginning in cycle 11 and especially 12 does not allow embryos to survive past cellularization (cycle 14).

In wild-type embryos, this is avoided by building furrows in two phases, Ingression I and Ingression II, with a Stabilization period in between (Xie and Blankenship, 2018). *spg* knockdown does not affect this biphasic nature of furrow ingression, as each cycle maintains both ingression periods as well as a measurable stabilization phase that is not significantly different in duration than wild-type. However, the rate of ingression that *spg* furrows can reach in any given ingression phase is slower than wild-type beginning in cycle 12, when furrow depths begin to fall significantly behind those in wild-type embryos (Fig. 1). This shows that Spg is not affecting only certain mechanisms of furrow ingression, but is acting on all phases. Further evidence of this can be seen in the width of the furrows. As furrows transition from the mechanism of Ingression I to that of Ingression II, furrows change in morphology from broad and diffuse to very sharp (Xie and Blankenship, 2018). In *spg* embryos, a defect in furrows in addition to shortened length is that they are very broad throughout cycles 10-13. However, although significantly wider than wild-type furrows, they maintain the

transition to thinner furrows as the cycle moves into the Ingression II phase (Fig. 6).

Together, these data show that *spg* furrow ingression is still occurring in a predictable

pattern but is severely disrupted in every aspect of this pattern, suggesting Spg as a

master regulator over the overall process of furrow ingression. As Spg was found to

impact mainly Actin cap components, this further implies the importance of the cap to

proper furrow ingression.

Spg contributions to F-actin populations

       F-actin levels are dramatically reduced both on apical caps and on furrows in *spg*

embryos. As these are two distinct populations of Actin—branched on the cap and linear

on the furrow—this gives the possibility that Spg could regulate both pathways of Actin

polymerization. Reducing linear F-actin populations through *dia* knockdown results in a

shortened furrow phenotype reminiscent of what is seen in *spg* (Fig. 4). However, several

characteristics of *dia* furrows indicate they are being controlled by a separate mechanism

than those in *spg* disrupted embryos. First, furrows are able to reach a significantly longer

maximum depth of 3.5 µm, reducing the occurrence of mitotic defects. To achieve this

greater length, *dia* furrows ingress at maximal rates closer to those in wild-type. In the

Ingression I phases of cycle 12-13, when *spg* furrow ingression is slow, *dia* maximal

ingression rates are slightly higher than or equal to wild-type furrows, showing no

significant difference. It is only in Ingression II phases that *dia* maximum ingression rates

fall behind wild-type (Fig. 4). Similarly, *dia* furrow morphologies are thinner and sharper

than those in *spg* throughout cycles 10-13, and are thinner than or not significantly

different from wild-type furrows during Ingression I phases. It is only in Ingression II

phases that *dia* furrows are significantly wider than wild-type, although they do still

transition to a sharper morphology than in respective Ingression I phases (Fig. 6). In

contrast to Spg, which is needed for both Ingression I and Ingression II, Dia appears more

important for Ingression II phases that are responsible for the bulk of a cycle's maximum

furrow length.

When branched F-actin networks are reduced through *arpc4* knockdown, the

resulting phenotype is more closely related to a *spg* phenotype. Furrows in *arpc4*

embryos reach a maximum length of 2.1 µm, the same as in *spg*. Maximum ingression

rates of these furrows also mimic a *spg* phenotype. *arpc4* furrows ingress at a maximum

rate equal to that of *spg* furrows during the Ingression I phase of cycles 11-13, when *dia*

maximum ingression rates are greater than or equal to wild-type. Consistent with the

biphasic defects seen in *spg*, the maximum ingression rates during Ingression II phases

when *arpc4* is disrupted are also significantly slower than wild-type and not significantly

different than in *spg* embryos (Fig. 5). These furrows also maintain a *spg*-like broad

furrow morphology, and *arpc4* furrows are significantly wider than wild-type in every

syncytial ingression phase (Fig. 6). As branched F-actin networks are primarily involved

in apical Actin caps, disrupting *arpc4* also severely affects caps. While cap-like structures

are produced with *arpc4* shRNA, they are strongly reduced in both size and Actin

intensity, similar to the structures produced in *spg* embryos (Fig. 6). Together, the many

similarities between both furrows and caps in *arpc4* and *spg* backgrounds indicate Spg is

an upstream regulator of Arp2/3.

Regulation of Arp2/3

As previously described, many factors are involved in activating, enhancing, and otherwise regulating Arp2/3 activity, including Scar, Coronin, DPod1, and Cortactin. Each of these can be found, unsurprisingly, on the apical caps where Arp2/3 mediated branched F-actin is prominent. These regulators are all disrupted to varying degrees on caps when *spg* is knocked down. Each is reduced to the areas of the small residual cap-like structures, with any remaining protein being mislocalized as random puncta throughout the cytoplasm (Fig. 7). Within these cap-like structures, Scar is the most severely diminished; from cycle 10-13, Scar intensity is on average 70% reduced from wild-type. This is likely the biggest contributing factor to the complete mislocalization of Arp2/3 in *spg* embryos as Scar is the main activator of Arp2/3 in *Drosophila* at these stages. Coronin is the next most severely affected factor; Coronin levels on the residual caps are on average 67% lower than on wild-type caps followed by Coronin-family protein DPod1 with a 49% reduction over cycles 10-13. This is also significant as Coronin has been found to directly regulate Arp2/3 in other systems. One regulator that does not appear to require Spg for localization to the apical cap, however, is Cortactin. While Cortactin is only present on the small residual structures in *spg* embryos, it is present on these structures in significantly increased intensity levels, suggesting proper localization to this more compact area leading to a brighter appearance (Fig. 7).

Interestingly, each of these regulators normally also localizes to the basal periphery of caps, where the cap structure meets the apical end of the ingressing furrows. Their presence extends onto furrows 2-3 µm, approximately the length of a typical *spg* furrow. While phenotypes of these proteins on the apical cap varies with *spg* disruption,

the effect on their localization to the furrows is ubiquitous. When *spg* is knocked down, Scar, Coronin, DPod1, and Cortactin are all absent on the furrows (Fig. 7). Instead, in the area of the furrows these proteins can be found as randomly dispersed cytoplasmic puncta. *spg* embryos produce short furrows up to 2 µm independently of Arp2/3, as Arp and its regulators are all mislocalized away from the furrows in these embryos. However, these furrows do not extend past the point where these proteins would normally be. This suggests that a population of Arp2/3 branched F-actin is critical on the apical furrows to support Dia linear F-actin and membrane furrows extending beyond this point.

Spg DOCK function

As a DOCK3/4 homologous protein, Spg is predicted to be a Rac1 and/or Rap1 GEF. Indeed, there are several reports of Spg acting as a GEF for both of these GTPases later in *Drosophila* development (Biersmith et al., 2011; Eguchi et al., 2013; Morishita et al., 2014; Biersmith et al., 2015). In syncytial stages, Rac1 and Rap1 do not seem to be essential to furrow formation as typical furrow defects are not observed. *rap1* and *rac1* embryos develop normally beyond syncytial stages, and furrow lengths in *rac1* embryos are not significantly different from wild-type. Furthermore, both proteins correctly localize to the plasma membrane in *spg* embryos at similar levels as in wild-type. If Spg was acting as a GEF in this stage, it would be expected that when Rac1 or Rap1 function was disrupted, furrows would more closely phenocopy those seen in *spg* embryos. Further, while the Rac1/Rap1 measured on membrane furrows was universally tagged and may have been GDP-bound and therefore inactive, it is still reasonable to expect to find decreased levels in a *spg* background to account for less active, GTP-bound, protein.

Given this, it seems that Spg does not function as a GEF in syncytial stages. Spg is a very large protein, ~2002 amino acids, and has several non-GEF domains including an SH3 domain, Armadillo-like helical domain, and undefined regions. SH3 and Armadillo helical domains often facilitate protein-protein interactions and could be the more important regions of Spg being used at this stage of development. Spg may be acting as a scaffolding protein to bring the many components of the Arp2/3 pathway that it regulates together to the caps and furrows.

Future Directions

To further understand Spg's involvement in Arp2/3 directed F-actin polymerization on syncytial caps and furrows, it would be interesting to compare phenotypes when Arp2/3 regulators are disrupted. If Spg is truly required for regulators such as Scar, Coronin, and DPod1 to localize to caps and furrows, and if their localization is truly required for furrow ingression, it would be expected that knocking down these proteins would produce a *spg*-like phenotype.

In addition, it is still unknown what mechanism is responsible for the short, 2-3 µm furrows that are successfully produced when F-actin networks are perturbed. A membrane trafficking pathway involving RalA, the exocyst complex, and Rab8 is known to facilitate membrane addition to the furrows, and these components were found to be unaffected in *spg* embryos. It has previously been shown that when this pathway itself is disrupted, furrows do not form. Therefore, it is possible that this pathway is responsible for initiating the first few microns of a furrow. Since there are still minimal amounts of F-actin on the furrows in *spg* embryos, this idea could be further explored by more severely

reducing Actin and testing whether short furrows can form, and whether RalA and Rab8 localize properly to the shortened furrows.

Finally, further testing must be done to confirm that Spg does not act as a GEF in syncytial stages as it does in so many others, especially considering the role of Rac1 as an upstream activator of Scar-Arp2/3 pathways. To do this, a construct could be created in which all the GEF-related domains of Spg are removed, leaving only the SH3, Armadillo helical, and undefined regions. If scaffold activity is the main function of Spg, these domains should be sufficient to carry out its function. This construct should then be able to rescue the *spg* phenotype and allow proper localization of Arp regulators and Arp2/3, leading to adequate furrow ingression.

References

Afshar K, Stuart B, Wasserman A. Functional analysis of the Drosophila diaphanous FH protein in early embryonic development. Development. 2000;127(9):1887-1897.

Bharathi V, Pallavi SK, Bajpai R, Emerald BS, Shashidhara LS. Genetic characterization of the Drosophila homologue of coronin. Journal of Cell Science. 2003;117:1911-1922.

Biersmith B, Liu ZC, Bauman K, Geisbrecht ER. The DOCK protein sponge binds to ELMO and functions in Drosophila embryonic CNS development. PLoS ONE. 2011;6: e16120.

Biersmith B, Wang ZH, Geisbrecht ER. Fine-Tuning of the Actin Cytoskeleton and Cell Adhesion During Drosophila Development by the Unconventional Guanine Nucleotide Exchange Factors Myoblast City and Sponge. Genetics. 2015;200(2):551-567.

Bogdan S, Schultz J, Grosshans J. Formin' cellular structures: Physiological roles of Diaphanous (Dia) in actin dynamics. Communicative & Integrative Biology. 2013;6(6): e27634.

Cao J, Crest J, Fasulo B, Sullivan W. Cortical actin dynamics facilitate early stage centrosome separation. Current biology: CB. 2010;20(8):770-776.

Côté JF, Vuori K. Identification of an evolutionarily conserved superfamily of DOCK180-related proteins with guanine nucleotide exchange activity. Journal of Cell Science. 2002;115(24):4901-4913.

Côté JF, Vuori K. GEF what? Dock180 and related proteins help Rac to polarize cells in new ways. Trends in cell biology. 2007;17(8):383-393.

Daly RJ. Cortactin signaling and dynamic actin networks. Biochem J. 2004;382:13-25.

Eguchi K, Yoshioka Y, Yoshida H, Morishita K, Miyata S., Hiai H, Yamaguchi M. The Drosophila DOCK family protein sponge is involved in differentiation of R7 photoreceptor cells. Exp. Cell Res. 2013;319:2179–2195.

Fabrowski P, Necakov AS, Mumbauer S, Loeser E, Reversi A, Streichan S, Briggs JAG, De Renzis S. Tubular endocytosis drives remodelling of the apical surface during epithelial morphogenesis in Drosophila. Nat. Commun. 2013;4,2244.

Figard L, Wang M, Xheng L, Golding I, Sokac AM. Membrane Supply and Demand Regulates F-Actin in a Cell Surface Reservoir. Dev Cell. 2016;37(3):267-278.

Figard L, Xu H, Garcia HG, Golding I, Sokac AM. The plasma membrane flattens out to fuel cell-surface growth during Drosophila cellularization. Dev Cell. 2013;27(6):648-655.

Foe VE, Alberts BM. Studies of nuclear and cytoplasmic behaviour during the five mitotic cycles that precede gastrulation in Drosophila embryogenesis. Journal of cell science. 1983;61(1):31–70.

Gadea G, Blangy A. Dock-family exchange factors in cell migration and disease. Eur J Cell Biol. 2014;93(10-12):466-477.

Helbig KL, Mroske C, Moorthy D, Sajan SA, Velinov M. Biallelic loss-of-function variants in DOCK3 cause muscle hypotonia, ataxia, and intellectual disability. Clin Genet. 2017;92:430–433.

Holly RM, Mavor LM, Zuo Z, Blankenship JT. A rapid, membrane-dependent pathway directs furrow formation through RalA in the early Drosophila embryo. Development. 2015;142(13):2316–28.

Iwata-Otsubo A, Ritter AL, Weckselbatt B, Ryan NR, Burgess D, Conlin LK, Izumi K. DOCK3-related neurodevelopmental syndrome: Biallelic intragenic deletion of DOCK3 in a boy with developmental delay and hypotonia. Am J Med Genet Part A. 2018;176A:241-245.

Laurin M, Côté JF. Insights into the biological functions of Dock family guanine nucleotide exchange factors. Genes Dev. 2014;28:533–547.

Machesky LM, Gould KL. The Arp2/3 complex: a multifunctional actin organizer. Curr. Opin. Cell Biol. 1999;11:117-121.

Mavor LM, Miao H, Zuo Z, Holly RM, Xie Y, Loerke D, Blankenship JT. Rab8 directs furrow ingression and membrane addition during epithelial formation in Drosophila melanogaster. Development. 2016;143(5):892-903.

Mazumdar A, Mazumdar M. How one becomes many: blastoderm cellularization in Drosophila melanogaster. Bioessays. 2002;24(11):1012–22.

Morishita K, Ozasa F, Eguchi K, Yoshioka Y, Yoshida H, Hiai H, Yamaguchi M. Drosophila DOCK Family Protein Sponge Regulates the JNK Pathway during Thorax Development. Cell Struct. Funct. 2014;39(2):113-124.

Postner MA, Miller KG, Wieschaus EF. Maternal effect mutations of the sponge locus affect actin cytoskeletal rearrangements in Drosophila melanogaster embryos. J. Cell Biol. 1992;119:1205–1218.

Rikhy R, Mavrakis M, Lippincott-Schwartz J. Dynamin regulates metaphase furrow formation and plasma membrane compartmentalization in the syncytial Drosophila embryo. Biol Open. 2015;4(3):301-311.

Rothenberg ME, Rogers SL, Vale RD, Jan LY, Jan YN. Drosophila Pod-1 Crosslinks Both Actin and Microtubules and Controls the Targeting of Axons. Neuron. 2003;39(5):779-791.

Rybakin V, Clemen CS. Coronin proteins as multifunctional regulators of the cytoskeleton and membrane trafficking. BioEssays. 2005;27:625-632.

Schejter E, Wieschaus E. Functional elements of the cytoskeleton in the early Drosophila embryo. Annual review of cell biology. 1993;9(1):67–99.

Sokac AM, Wieschaus E. Zygotically controlled F-actin establishes cortical compartments to stabilize furrows during Drosophila cellularization. Journal of cell science. 2008;121(11):1815–24.

Stevenson V, Hudson A, Cooley L, Theurkaud WE. Arp2/3-Dependent Pseudocleavage Furrow Assembly in Syncytial Drosophila Embryos. Current Biology. 2002;12(9):705-711.

Sullivan W, Fogarty P, Theurkauf W. Mutations affecting the cytoskeletal organization of syncytial Drosophila embryos. Development. 1993;118(4):1245–54.

Sullivan W, Theurkauf WE. The cytoskeleton and morphogenesis of the early Drosophila embryo. Curr. Opin. Cell Biol. 1995;7,18-22.

Ueda S, Fujimoto S, Hiramoto K, Negishi M, Katoh H. Dock4 regulates dendritic development in hippocampal neurons. J. Neurosci. Res. 2008;86:3052-3061.

Xie Y, Blankenship JT. Differentially-dimensioned furrow formation by zygotic gene expression and the MBT. Desplan C, ed. PLoS Genetics. 2018;14(1):e1007174.

Yajnik V, Paulding C, Sordella R, McClatchey AI, Saito M, Wahrer DCR, Reynolds P, Bell DW, Lake R, van den Heuvet S, Settleman J, Haber DA. Dock4, a GTPase Activator, Is Disrupted during Tumorigenesis. Cell. 2003;112(5):673-684.

Zallen JA, Cohen Y, Hudson AM, Cooley L, Wieschaus E, Schejter ED. SCAR is a primary regulator of Arp2/3-dependent morphological events in Drosophila. JCB. 2002;156(4):689-701.